AUTOIMMUNITY

Disrupted degradative sorting of TLR7 is associated with human lupus

Harshita Mishra[1], Claire Schlack-Leigers[2], Ee Lyn Lim[1], Oliver Thieck[1], Thomas Magg[3], Johannes Raedler[3], Christine Wolf[5], Christoph Klein[3], Helge Ewers[2], Min Ae Lee-Kirsch[5], David Meierhofer[4], Fabian Hauck[3]*, Olivia Majer[1]*

Hyperactive TLR7 signaling has long been appreciated as driver of autoimmune disease in mouse models. Recently, gain-of-function mutations in TLR7 were identified as a monogenic cause of human lupus. TLR7 is an intracellular transmembrane receptor, sensing RNA breakdown products within late endosomes. Here, we show that endosome dysfunction leads to unrestricted TLR7 signaling and is associated with human lupus. The late endosomal BORC complex together with the small GTPase Arl8b controls intracellular TLR7 levels by regulating receptor turnover. This requires a direct interaction between the TLR7-associated trafficking factor Unc93b1 and Arl8b. We identified an UNC93B1 mutation in a patient with childhood-onset lupus, which results in reduced BORC interaction and endosomal TLR7 accumulation. Therefore, a failure to control TLR7 turnover is sufficient to break immunological tolerance to nucleic acids. Our results highlight the importance of an intact endomembrane system in preventing pathological TLR7 signaling and autoimmune disease.

INTRODUCTION

Nucleic acid-sensing toll-like receptors (TLRs), including the RNA sensor TLR7, are responsible for the difficult task of efficiently recognizing and responding to foreign genomic material, while maintaining tolerance to self-derived nucleic acids (*1*). This discrimination is achieved through the intracellular localization of TLR7 within late endosomes, which ensures effective sensing of released RNA from ingested pathogens but limits the exposure of TLR7 to self-derived ligands. To reach late endosomes and become signaling competent, TLR7 relies on a complex interplay between transport mechanisms, membrane interactions, and proteolytic processing in acidic endosomal compartments (*2*–*4*). Mechanistic studies on TLR7 gain-of-function have primarily focused on hard-wired mutations in either TLR7, or its associated trafficking factor Unc93b1. Known sources for hyperactive TLR7 include *Tlr7* gene duplications (*5*–*7*), mutations increasing ligand affinity (*8*) or Unc93b1 mutations releasing the brake on TLR7 signaling (*9*–*11*). However, regulatory mechanisms of TLR7 activity involving the receptor-containing organelle or endosome-related trafficking processes have not been described.

Late endosomes/lysosomes, from which TLR7 signals, are the main degradative organelle in eukaryotic cells that also serve as a central coordinator and signaling hub of the cell (*12*). Accessory and transmembrane proteins assemble in functional complexes at the endosomal membrane to orchestrate the response of key cellular processes to environmental cues. One of these complexes is BLOC1-related complex (BORC), a critical regulator of lysosome biology that controls lysosome positioning within the cytoplasm, as well as vesicle fusion of late endosomes and autophagosomes with lysosomes (*13*). BORC is composed of eight conserved subunits that assemble on the cytosolic surface of the endosome (*14*). The complex recruits the small Arf1-like GTPase Arl8b that serves as an adaptor for connecting BORC to different downstream protein machineries to mediate vesicle trafficking and fusion.

Here, we report that BORC and Arl8b are both required to maintain immunological tolerance by regulating the homeostatic turnover of TLR7. BORC-mediated degradative sorting, thereby, controls the intracellular level of functional TLR7 and limits the self-reactivity to nucleic acids. To coordinate lysosomal degradation of TLR7, the BORC complex physically interacts with TLR7 through Unc93b1. We describe a patient with a heterozygous UNC93B1 mutation that weakens this interaction, leading to endosomal TLR7 accumulation associated with childhood-onset lupus.

RESULTS

The BORC-Arl8b complex restricts TLR7 signaling

The BORC complex has been identified and best studied in epithelial cells. In Hela cells, loss of BORC-Arl8b abrogates anterograde lysosomal transport and results in the clustering of late endosomes/lysosomes in the perinuclear region (*14*), whereas overexpression relocates late endosomes into the cell periphery (*15*). We first confirmed these results by either knocking down BORC subunit 5 (Borcs5) or overexpressing Arl8b (Fig. 1A). To examine how these endosome manipulations would affect endosomal TLR signaling, we co-expressed and stimulated TLR7 in these cells. BORC-depleted Hela cells showed enhanced TLR7 signaling, as measured by increased induction of endogenous *IL-8* in response to R848 stimulation (Fig. 1B). In contrast, overexpression of Arl8b suppressed TLR7 signaling, without affecting protein levels (Fig. 1C). As gain-of-function TLR7 is a known driver of autoimmune disease (*8*) and juxtanuclear endosome clustering has been described in inflammatory pathologies, including neurodegenerative and lysosomal storage disorders (*16*–*18*), we further investigated the BORC-mediated restriction of TLR7 signaling.

To test if BORC would limit TLR7 signaling in immune cells, we deleted Borcs5 and Arl8b in mouse macrophages derived from

[1]Max Planck Institute for Infection Biology; Berlin, 10117, Germany. [2]Institute for Chemistry and Biochemistry, Freie Universität Berlin; Berlin, 14195, Germany. [3]Department of Pediatrics, Dr. von Hauner Children's Hospital, University Hospital, Ludwig-Maximilians-Universität München; Munich, 80337, Germany. [4]Max Planck Institute for Molecular Genetics; Berlin, 14195, Germany. [5]Department of Pediatrics, Medizinische Fakultät Carl Gustav Carus, Technische Universität Dresden; Dresden, 01307, Germany.
*Corresponding author. Email: majer@mpiib-berlin.mpg.de (O.M.); fabian.hauck@med.uni-muenchen.de (F.H.)

Hoxb8-immortalized myeloid progenitor cells (hereafter referred to as 'Hoxb8 macrophages'). The morphology and function of these cells resembles very closely bone marrow-derived primary macrophages, and can be considered a primary-like cell system. Lentiviral CRISPR/Cas9-mediated knockout of Borcs5 or Arl8b greatly enhanced TLR7 signaling, as evidenced by higher production of TNF (Fig. 1D). The hyperresponsiveness was specific to TLR7, and did not apply to TLR9. As expected, surface TLR4 and TLR2 signaling were not affected by the endosome manipulation. The TLR7 hyperresponsiveness was dose-dependent and best demonstrated at suboptimal ligand concentrations (Fig. 1E). We validated these finding in two independent Borcs5 KO lines targeted with different guide RNAs (Fig. 1E) and

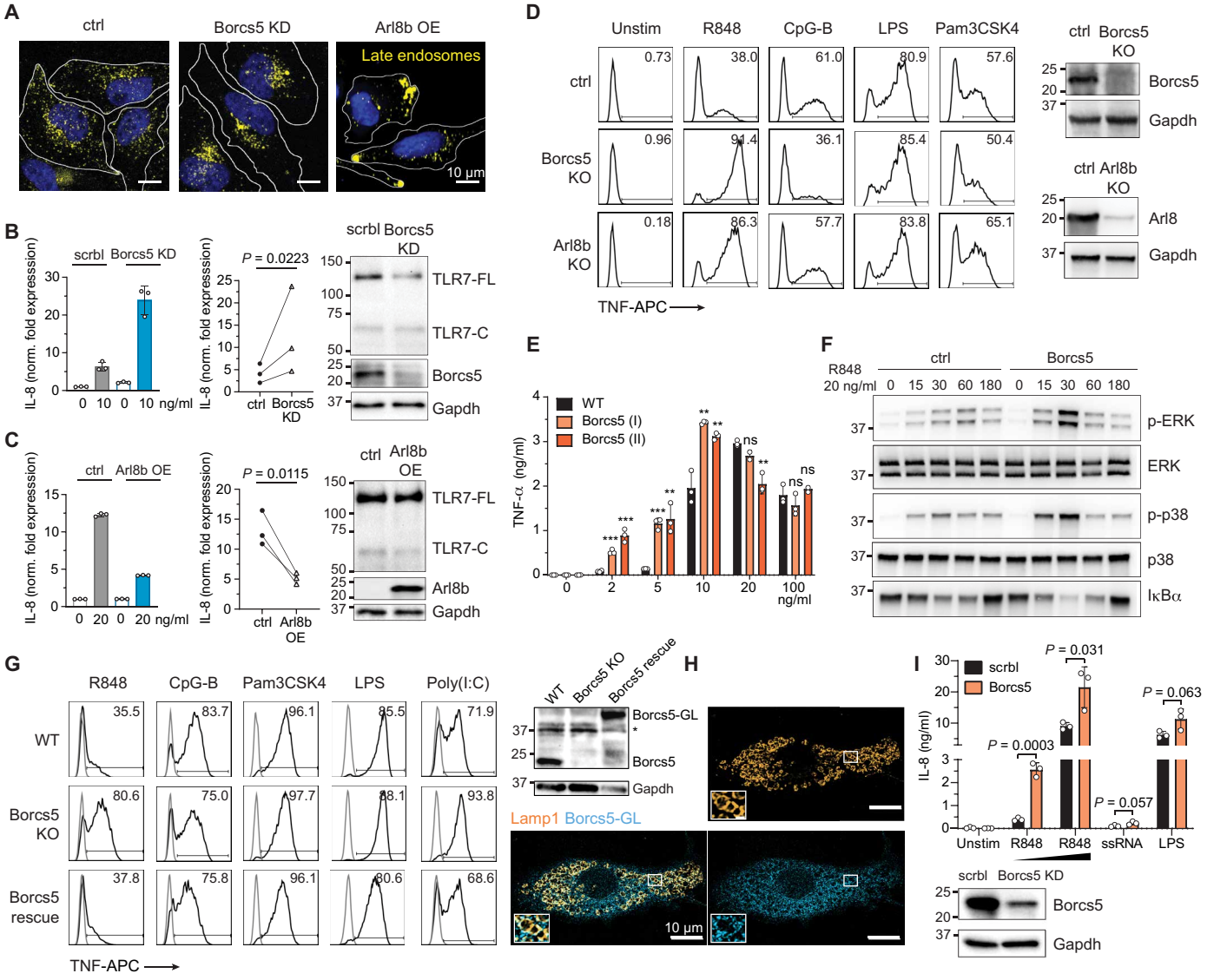

Fig.1. BORC-Arl8b restricts TLR7 signaling in human and mouse macrophages. (**A**) Endosomes of Hela cells were loaded with AlexaFluor 488-dextran and transfected with either siRNA against Borcs5 or an Arl8b expression plasmid. Representative images showing the repositioning of late endosomes. (**B**) Hela cells were co-transfected with TLR7-HA and siRNA against Borcs5. *IL8* gene induction was quantified by qPCR after 2 hours stimulation with R848. Bar graph shows a representative experiment. Dot plot shows pooled data of $N = 3$; ratio paired *t* test, two-tailed. Western blots show TLR7-HA expression. C: cleaved, FL: full-length. (**C**) Hela cells were co-transfected with TLR7-HA and Arl8b and treated as in (B). Graphs displayed and analyzed as in B. (**D**) Intracellular TNF staining of indicated Hoxb8 macrophage lines with R848 (10 ng/ml), CpG-B (300 nM), LPS (25 ng/ml) or Pam3CSK4 (50 ng/ml). Representative data of $N = 5$. Western blots show KO validations. (**E**) TNF ELISA of two Borcs5 KO Hoxb8 macrophages lines targeted with two separate guides after 8 hours stimulation with increasing concentrations of R848. Representative data ($n = 3$) of $N = 5$; unpaired *t* test, two-tailed. $^{**}P < 0.01$ and $^{***}P < 0.001$. (**F**) Immunoblot of phosphorylated P-p38, P-ERK and IκBα of Hoxb8 macrophages stimulated with R848 for the indicated times. Representative data of $N = 3$. (**G**) Intracellular TNF staining of indicated Raw246.7 macrophage lines with R848 (10 ng/ml), CpG-B (300 nM), Pam3CSK4 (50 ng/ml), LPS (25 ng/ml), or PolyIC (500 ng/ml). Western blots show KO validation and rescue (* unspecific band). Representative data of $N = 3$. (**H**) Representative image of Raw246.7 expressing Borcs5-GreenLantern (GL) stained for GFP and Lamp1. (**I**) IL8 ELISA of Borcs5 knock-down THP1 macrophages after overnight stimulation with increasing doses of R848 (2.5 and 5 ng/ml), ssRNA (5 µg/ml), and LPS (50 ng/ml). Representative data ($n = 3$) of $N = 2$; unpaired *t* test, two-tailed. Western blot shows knock-down efficiency.

when knocking out other BORC subunits, including Borcs6 and Borcs7 (fig. S1A). The enhanced TNF response could be reverted to WT levels by reintroducing Borcs5 or Arl8b into the respective KO lines (fig. S1B).TLR7 was also more active in response to its physiological ligand ssRNA (fig. S1C). BORC deletion led to increased phosphorylation of the MAPKs p38 and ERK, and stronger degradation of IκBα downstream of TLR7 receptor activation (Fig. 1F), which was not observed when stimulating TLR9 (fig. S1D). As all activated pathways returned to baseline with similar kinetics, we excluded the activity of negative feedback mechanisms. Enhanced TLR7 signaling was not a result of enriched levels of signaling molecules within the pathway, as proteomic analysis revealed normal levels of these proteins in BORC-deleted Hoxb8 macrophages (fig. S1E).

To verify the phenotype in an independent macrophage system, we knocked out Borcs5 in murine Raw264.7 macrophages through Cas9-RNP delivery and obtained two independent clones. In both BORC-deleted clones, TLR7 signaling was enhanced, whereas TLR9 signaling was slightly reduced (Fig. 1G and fig. S1F). Again, surface TLR2 and TLR4 were unaffected. The TLR7 hyperresponse was not restricted to the NFκB signaling pathway (TNF), but also extended to the type I interferon signaling branch (*Ifnb*) (fig. S1G). We extended our analysis to TLR3, another endosomal RNA sensor, and also found this receptor slightly more active in response to Poly-IC stimulation, although not to the same magnitude as TLR7. All observed TLR signaling phenotypes could be rescued by reintroducing Borcs5 (Fig. 1G). Both mouse Borcs5 isoforms were able to rescue the TLR7 hyperresponse (fig. S1, H and I), even though only isoform 2 can be myristoylated, a modification believed to mediate lysosomal membrane attachment (*14*). Imaging confirmed that both isoforms localized to late endosomes (Fig. 1H and fig. S1J), suggesting that myristoylation is not the only way to anchor Borcs5 to endosomal membranes. We also extended our analysis to mouse Hoxb8 progenitor-derived dendritic cells. These cells express CD11b, CD11c and various amounts of MHC-II after differentiation (fig. S1K). Similar to.

Hoxb8 macrophages, we observed a specific enhancement of TLR7 signaling in Borcs5-deficient dendritic cells, confirming this regulation across multiple myeloid cell lineages (fig. S1K).

Finally, we verified our findings in human THP-1 macrophages. siRNA-mediated knockdown of Borcs5 in PMA-differentiated THP-1 macrophages corroborated the increased response to R848 and ssRNA40 seen in mouse macrophages, without affecting LPS signaling. (Fig. 1I). As R848 is a dual ligand for both human TLR7 and TLR8, we additionally stimulated THP-1 macrophages with the TLR8-specific agonist TL8–506. Corroborating results with TLR7, TLR8 stimulation with TL8–506 yielded higher responses in Borcs5 knock-down THP-1 cells, suggesting that BORC regulates both TLR7 and TLR8 (fig. S1L).

These data show that the late endosomal BORC-Arl8b complex restricts TLR7/8 signaling in mouse and human macrophages, with minor effects on TLR3 and TLR9.

BORC deficiency has no effect on endosome positioning in macrophages

As BORC deficiency induces striking endosome clustering in epithelial cells, we next examined endosome positioning in macrophages. In contrast to Hela cells, endosomes in Arl8b- or Borcs5-deficient Hoxb8 macrophages did not collapse into the perinuclear region (Fig. 2A). To assess potential small differences in localization, we quantified the radial distribution of Lamp1$^+$ late endosomes/lysosomes. There were no significant differences in the Lamp1 distribution in Borcs5, Borcs7 or Arl8b KO Hoxb8 macrophages compared to control cells. (Fig. 2B and fig. S2A). Furthermore, we did not observe any differences in endosome positioning after TLR7 stimulation (fig. S3). One explanation for the lack of clustering might be the sheer abundance of late endosomes within macrophages, a feature related to their physiological function of being professional phagocytes, which could impede the visualization of any additional clustering. Alternatively, the endosomal architecture of macrophages might follow different rules for vesicle trafficking than Hela cells.

We also assessed endosomal pH and proteolysis, as these are prerequisites for cleavage of endosomal TLRs to generate functional receptors (*2*). The overall proteolytic capacity of endosomes in BORC-deficient Hoxb8 macrophages did not differ from control cells, as shown by comparable degradation of internalized DQ-BSA, a fluid-phase lysosomal proteolysis sensor (Fig. 2C). Equal endocytic uptake of cells was verified with fluorescent dextran (Fig. 2D). Also, luminal pH did not differ, as measured by the mean fluorescent intensity of internalized pHrhodo, a lysosomal pH reporter (fig. S2B). To rule out differences in the overall number of late endosomes, we compared the amount of Lamp1 in KO and control Hoxb8 macrophages (fig. S2C).

We extended our analysis to Borcs5-deficient Raw264.7 macrophages and confirmed a similar endosome distribution with live-cell microscopy (Fig. 2E). To quantitatively assess the pH of single endosomes, we performed ratiometric fluorescence microscopy. The luminal pH of individual endosomes did not significantly differ between WT and KO cells (Fig. 2F and fig. S2D). As macrophages were plated on fibronectin-coated coverslips for this assay to improve cell spreading, we confirmed the hyperactive TLR7 response in Borcs5 KO cells on this coating (fig. S2E).

Lastly, we assessed autophagy in BORC-deficient macrophages, as autophagy has previously been linked to TLR regulation (*19*) and BORC promotes autophagy through facilitating the final fusion between autophagosome and lysosome (*20*). We did not detected differences in the basal level of LC3B-II or in the autophagic flux in Borcs5 KO Raw264.7 macrophages (fig. S2F); excluding a role for autophagy in the BORC-mediated restriction of TLR7 signaling.

In summary, macrophages lacking BORC exhibit no impairment in endosome positioning, proteolysis, endosomal pH, or basal autophagy. This distinguishes their characteristics from the phenotypes observed in BORC-deficient epithelial cells.

BORC controls TLR7 turnover

Since BORC deficiency did not visibly change endosome positioning, pH, proteolysis, or autophagy in macrophages, we compared the protein composition of endosomes from WT and Borcs5 KO Raw264.7 macrophages to identify other endosome-related processes that could functionally explain the TLR7 gain-of-function. First, we magnetically purified phagosomes from macrophages that had been fed iron beads and analyzed the phagosome proteome by mass spectrometry (Fig. 3A). Gene Set Enrichment Analysis revealed a broad dysregulation of the phagosomal compartment, with many lysosome-related proteins being reduced in Borcs5-depleted phagosomes, including cathepsins, DNASE2, NPC2, and degradative enzymes of complex lipids and carbohydrates, and others being enriched, such as Furin. (Fig. 3B and fig. S4A). In agreement with the enhanced signaling response, TLR7 and TLR3 were enriched in phagosomes from KO cells. Notably, there was also an enrichment of early endosomal markers and effector proteins involved in the Rab5-to-Rab7 conversion (*21*),

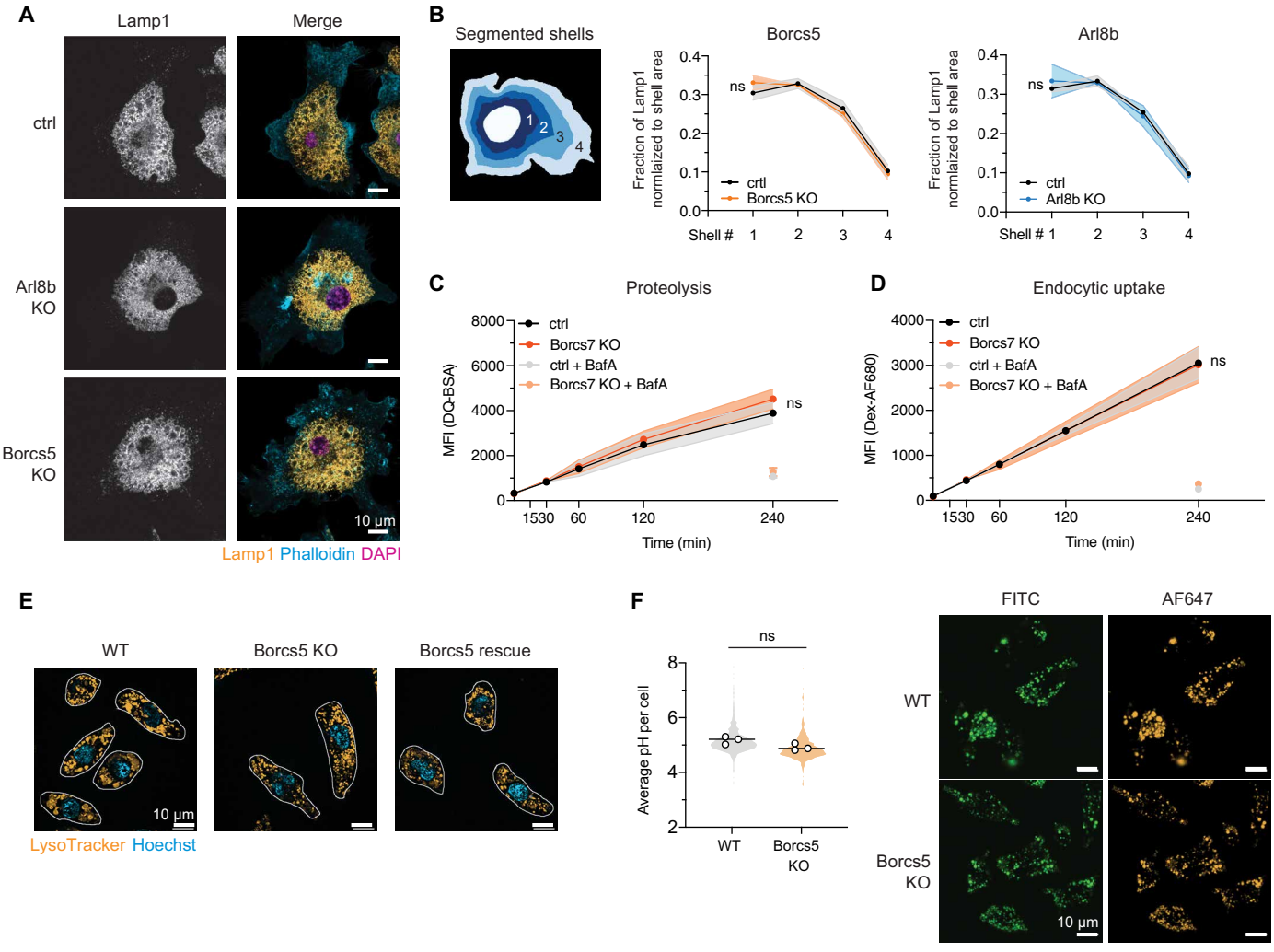

Fig.2. BORC deficiency does not alter endosome positioning, luminal pH or proteolysis in macrophages. (**A**) Indicated Hoxb8 macrophage lines were fixed and stained with anti-Lamp1, phalloidin, and DAPI to show endosome positioning. (**B**) Quantification of endosome radial distribution across segmented shells. Graphs show the fraction of late endosomes normalized per shell area. Pooled data from $N = 3$ (Borcs5) and $N = 2$ (Arl8b), shaded areas indicate the SD. (Total number of cells analyzed: WT: 241, Borcs5 KO: 243, Arl8b KO: 163); two-way ANOVA comparing variation between genotypes. (**C**) Quantification of the proteolytic capacity of endosomes by loading macrophages with the proteolysis reporter DQ-BSA Red for the indicated amounts of time. Bafilomycin A treatment served as negative control. Pooled data of $N = 3$, shaded areas indicate the SD; two-way ANOVA comparing variation between genotypes. (**D**) Quantification of endocytic uptake by loading macrophages with AlexaFluor680-Dextran for the indicated amounts of time. Data repeats and analysis as in (C). (**E**) Live cell images of indicated Raw246.7 macrophage lines fed with lysotracker, CellMask and Hoechst to show endosome positioning. (**F**) Lysosomal pH of WT and Borcs5 KO Raw246.7 macrophages were determined by ratiometric fluorescence microscopy. Pooled data from $N = 3$. Left: Dots represent means of independent experiments, shaded violin shows the variation of individual cells across all experiments; paired *t* test, two-tailed. ($n = 982$ WT & 884 Borcs5 KO cells). Right: Representative confocal images with identical acquisition and display settings.

suggesting a defect in endosome maturation (Fig. 3B). Early endosomal markers were not expected in these preparations, as beads were given enough time to traverse all the way into lysosomes. We independently validated these findings via Western blot and detected an accumulation of cleaved TLR7 and early endosomal markers EEA1 and Rab5 in phagosomes from Borcs5 KO macrophages, which returned back to WT levels in the rescue line (Fig. 3C). A similar accumulation of TLR7 and EEA1 was observed in phagosomes purified from Borcs7-deficient Hoxb8 macrophages (fig. S4B). The co-occurrence of both late and early endosomal markers in phagosome preparations from KO cells suggested either the existence of an unusual hybrid compartment, decorated by both markers, or a delay in phagocytosis with beads retained in early endosomes at the time of harvest. To distinguish between these two possibilities, we imaged individual bead-containing phagosomes in BORC KO cells after 3 hours of synchronized uptake. Beads taken up by WT cells were exclusively present in Lamp1$^+$ late endosomes/lysosomes. In Borcs5 KO macrophages, a sizable portion of beads were found within hybrid compartments, marked by both EEA1 and Lamp1 (Fig. 3D). In neither condition were beads detected in EEA1 single-positive early endosomes, ruling out delayed phagocytosis.

The existence of less mature hybrid compartments would predict increased TLR7 colocalization with early endosomal markers. We performed super-resolution microscopy quantifying the degree of

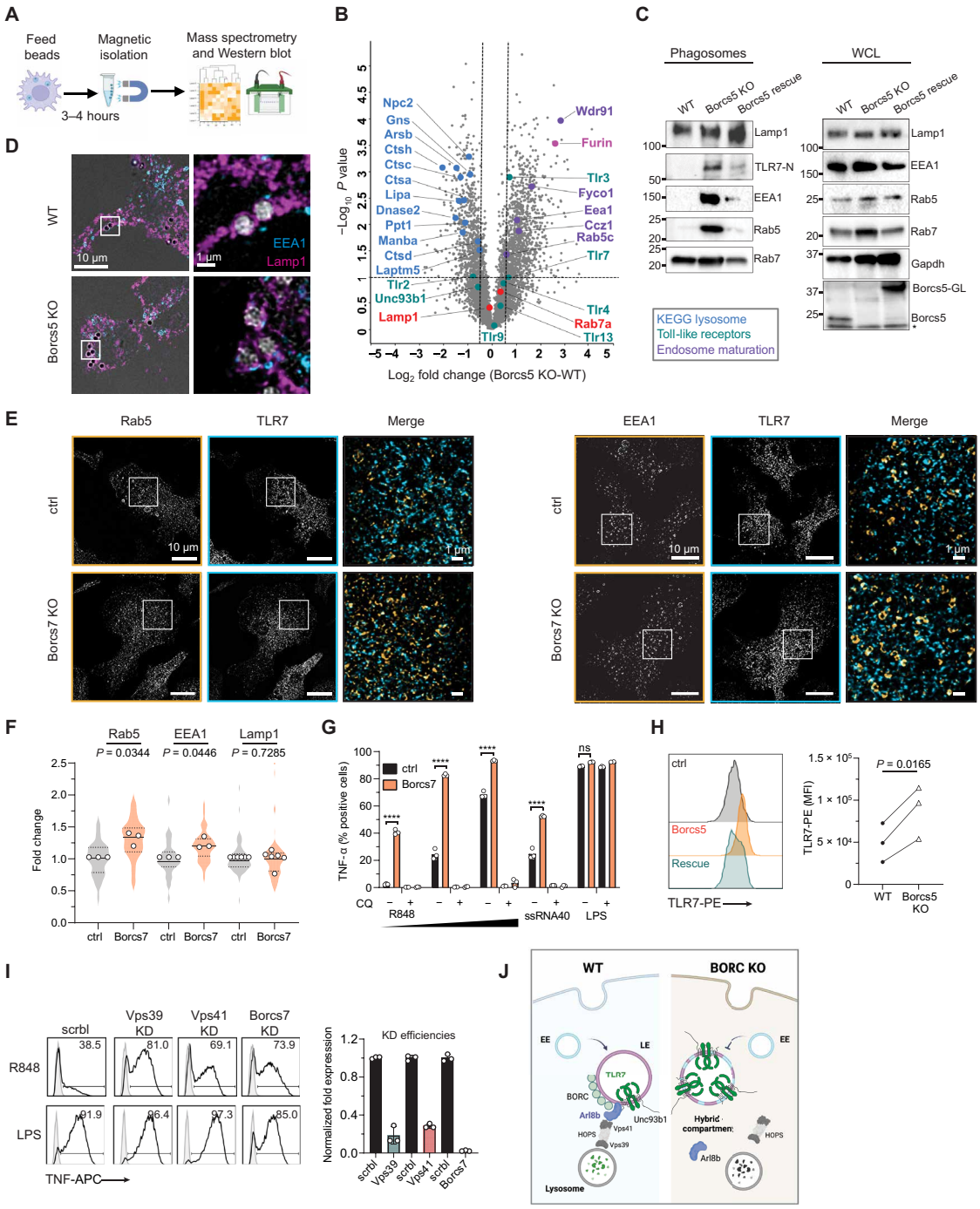

Fig.3. BORC controls endosome maturation and TLR7 turnover. (**A**) Phagosome purification workflow. (**B**) Volcano plot showing phagosome proteomics data ($n = 3$). The horizontal and vertical lines indicate a *P*-value of 0.1 and fold change of 1.5 respectively. Selected proteins are highlighted. (**C**) Western blot validation of phagosome preparations (* unspecific band). Representative data of $N = 3$. WCL: whole cell lysate. (**D**) EEA1 and Lamp1 staining of bead-containing phagosomes after 3 h of feeding to Raw267.5 macrophages. Representative images of $N = 2$. (**E**) Representative images of indicated Hoxb8 macrophage lines stained for endogenous TLR7 and either Rab5 or EEA1 and imaged on a structured illumination microscope. (**F**) Quantification of the colocalization between TLR7 and Rab5, EEA1, or Lamp1 in Borcs7 KO and ctrl Hoxb8 macrophages. Data is expressed as fold-change and pooled from $N = 3$. Dots represent means of independent experiments, shaded violin shows the variation of individual cells across all experiments; ratio paired *t* test, two-tailed. (**G**) Intracellular TNF staining of indicated Hoxb8 macrophage lines with R848 (2, 5, 10 ng/ml), ssRNA40/LyoVec (5 µg/ml), or LPS (25 ng/ml) in the presence or absence of chloroquine (CQ). Representative data ($n = 3$) of $N = 2$; unpaired *t* test, two-tailed. ****$P < 0.0001$. (**H**) TLR7 flow staining of indicated Raw264.7 macrophage lines. Histogram shows representative raw data; dot blot shows pooled data of $N = 3$; ratio paired *t* test, two-tailed. (**I**) Intracellular TNF staining of indicated knock-down Hoxb8 macrophages after 8 hours stimulation with R848 (5 ng/ml) and LPS (10 ng/ml). Representative data of $N = 3$. Right: qPCR validation of knock-down efficiencies of the presented experiment on the left. (**J**) Proposed model of how BORC-Arl8b controls TLR7 receptor levels and signaling activity. EE: early endosome, LE: late endosome.

TLR7 colocalization with the two early endosomal markers EEA1 and Rab5 (Fig. 3E and fig. S4C), as well as the late endosomal marker Lamp1. As predicted, there was higher overlap between TLR7 and Rab5/EEA1 in Borcs7 KO Hoxb8 macrophages, whereas colocalization with Lamp1 was unaffected (Fig. 3F). As the TLR7 distribution shifts towards less mature compartments with lower levels of major lysosomal proteases, we determined whether signaling was still dependent on acidification. Chloroquine treatment completely abrogated the TLR7 response in both WT and BORC KO macrophages (Fig. 3G).

Another reported function of the BORC-Arl8b complex is the regulation of vesicle fusion between late endosomes and lysosomes (*22*, *23*). We reasoned that by regulating lysosome fusion BORC would be able to control the turnover of membrane proteins targeted for lysosomal degradation, including TLR7. Indeed, we observed an overall accumulation of TLR7 protein in Borcs5-deficient macrophages by flow (Fig. 3H). In agreement with the MS dataset, we also observed a slight accumulation of TLR3, however, unlike TLR7, the data was less robust and did not reach significance (fig. S4D). The specificities of the anti-TLR7 and TLR3 antibodies were validated against KO controls (fig. S4E). To mediate the fusion between late endosomes and lysosomes, BORC-Arl8b recruits the mammalian homotypic fusion and protein sorting (HOPS) complex, a tethering complex regulating membrane fusion events with lysosomal membranes (*24*). Arl8b has been shown to directly interact with the HOPS subunit VPS41 (*25*), and phagosomes from BORCs5 KO macrophages showed a significant depletion of VPS41 (Data file S1). We therefore hypothesized that removal of HOPS complex components would recapitulate the TLR7 gain-of-function phenotype of BORC KO cells. Indeed, knock-down of the HOPS subunits Vps39 or Vps41 in Raw264.7 macrophages resulted in enhanced TLR7 signaling, providing independent confirmation on the role of impaired lysosome fusion (Fig. 3I). None of the knock-down conditions affected TLR4 signaling. Based on our findings, we propose a model in which the BORC-Arl8b complex safeguards the proper homeostatic turnover of TLR7 in resting cells. In the absence of Arl8b or BORC subunits, TLR7-containing late endosomes fuse less efficiently with lysosomes, resulting in a build-up of TLR7 within the endosomal compartment, which increases the cell's sensitivity for ligand stimulation (Fig. 3J).

BORC-Arl8b interacts with TLR7 through Unc93b1

Next, we determined whether BORC-Arl8b would directly interact with nucleic acid-sensing TLRs at endosomal membranes. We reasoned that an interaction would most likely occur through Unc93b1, as it is structurally wrapped around the TLR and provides abundant binding surfaces through its long cytosolic N- and C-terminal tails (*26*). We immunoprecipitated Flag-tagged Unc93b1 from Raw264.7 macrophages and observed an interaction with endogenous Arl8b and TLR7 (Fig. 4A). The interaction was independent of TLR7 stimulation but required functional Unc93b1 that reaches late endosomes, as the trafficking-deficient H412R mutant Unc93b1 (*27*) did not bind Arl8b (Fig. 4A). Alphafold multimer modeling predicted a putative interaction of Arl8b with the acidic patch (45–49 EEEEE) in the N terminus of Unc93b1, as well as additional regions including I317 in loop 6 (Fig. 4, B and C and fig. S5A). We introduced triple alanine mutations into the predicted Unc93b1 binding surfaces including surrounding areas and showed that these mutant alleles, when expressed in Raw264.7 macrophages, phenocopied the TLR7 hyperresponse observed in Arl8b or BORC KO macrophages (fig. S5B).

To test whether any of these regions mediate the association with Arl8b, we performed co-immunoprecipitation experiments. All tested Unc93b1 mutations showed a clear reduction in Arl8b binding (Fig. 4D), correlating well with the TLR7 hyperresponsiveness. One of the tested Unc93b1 alleles included the previously reported D34A mutation, which drives lupus-like disease in mice (*9*), indicating a potential involvement of BORC-mediated regulation for this mutation also. As none of the individual Unc93b1 mutants showed a complete loss of Arl8b binding, contact between multiple surfaces might be required for efficient binding.

After having mapped the interaction of Unc93b1 and Arl8b, we sought to determine which specific TLR-Unc93b1 complex would engage with the Arl8-BORC complex. HA-tagged TLR3, TLR7, and TLR9 were immunoprecipitated from separate Raw264.7 macrophage lines and probed for binding to Arl8b. Strikingly, only TLR7 pulled down Arl8b, whereas neither TLR3 nor 9 showed an interaction (Fig. 4E). The specific interaction with TLR7 can be explained by the fact that both TLR3 and 9 release from Unc93b1 once inside the endosome, whereas TLR7 remains associated (*28*). However, how BORC still influences the signaling of TLR3 without directly interacting with the receptors will require further investigation. To confirm the TLR7-Arl8b interaction at late endosomal membranes, we performed super-resolution imaging of cells labeled for endogenous TLR7, Arl8b, and Lamp1 (Fig. 4F). Antibody specificities against mouse TLR7 and Arl8b were confirmed using the respective KO lines (fig. S5C). In the absence of BORC, colocalization between Arl8b and TLR7 decreased (Fig. 4G), due to reduced recruitment of Arl8b to late endosomes (Fig. 4H and fig. S5D). Using Raw264.7 macrophages expressing Borcs5-GreenLantern, we also showed that TLR7 colocalizes with BORC at late endosomes (Fig. 4I), although in Co-IP experiments we had not been able to directly pull down BORC subunits with TLR7.

These data establish that BORC mediates TLR7 degradation through bridging TLR7/Unc93b1 with Arl8b and the HOPS complex at late endosomal membranes and that this interaction is important to restrict TLR7 signaling. BORC deficiency as well as mutations in Unc93b1 reducing the interaction with Arl8b/BORC both result in accumulation of TLR7. Based on these observations, we propose a dual function of BORC in this process: 1) a general function, in which BORC connects late endosomes with lysosomes for fusion, and 2) a specific function, in which BORC recognizes TLR7 (via Unc93b1) as cargo to be sorted into these lysosomes. To uncouple these two functions, we assessed endosome maturation in macrophage lines with reduced Unc93b1-Arl8b interactions, but otherwise harboring an intact BORC complex. As expected, endosome maturation was normal in cells expressing Unc93b1 mutations with reduced Arl8b interaction, indicated by the absence of early endosome markers on phagosome preparations (fig. S5E). These results demonstrate that even in the presence of functional BORC and normal endosome maturation, TLR7 still needs to be recognized by Arl8b/BORC as degradative cargo, as otherwise cells develop TLR7 hyperactivity.

Breaking the interaction between Arl8b and Unc93b1 causes human lupus

To extend the relevance of our findings to human pathophysiology, we analyzed patients with autoimmune disease and identified a young female with systemic lupus erythematosus (SLE) who harbored a monoallelic UNC93B1 mutation (Fig. 5A). The variant was inherited from her father, who had not yet come to medical attention (Fig. 5A). The

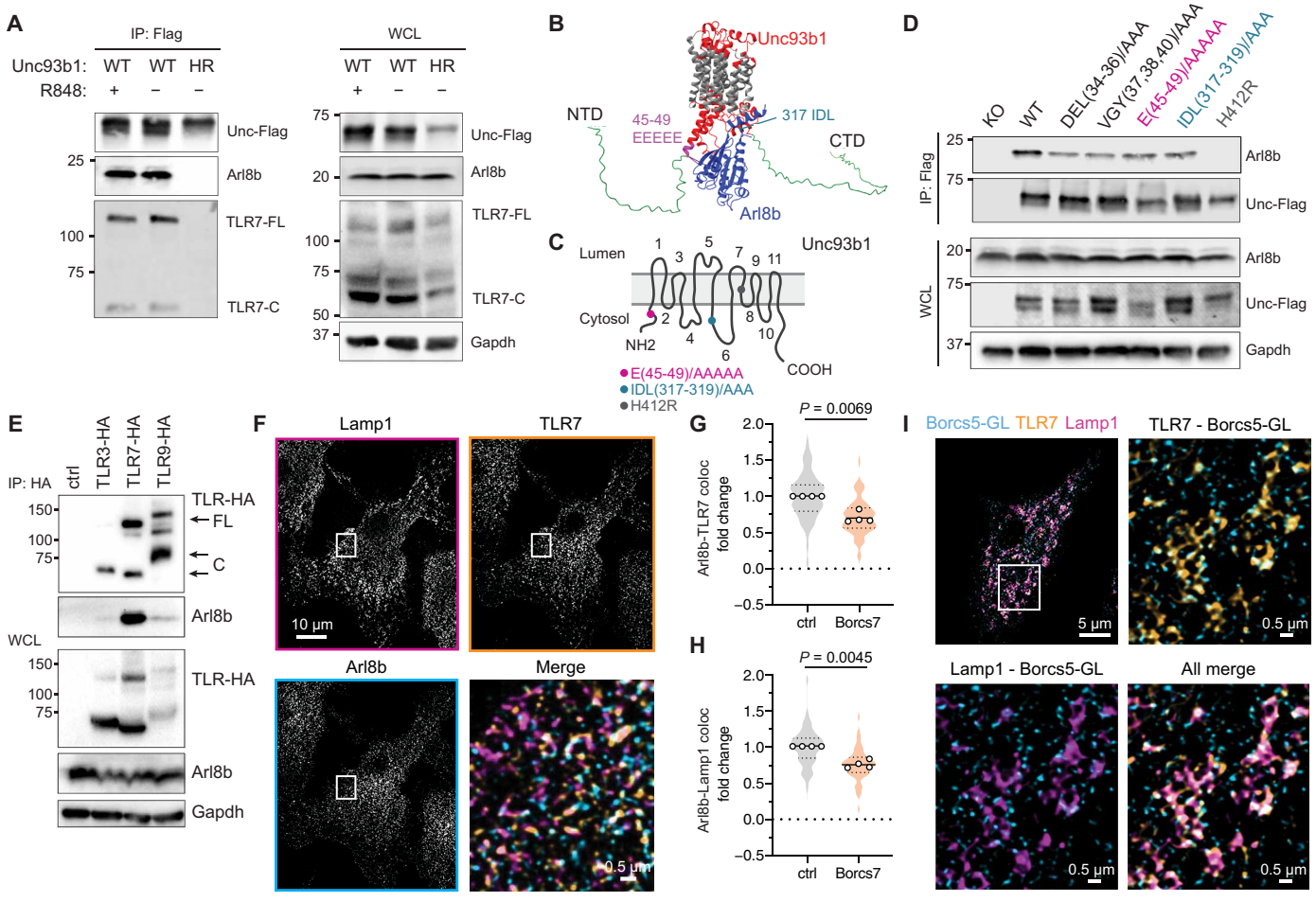

Fig.4. BORC-Arl8b interacts exclusively with the TLR7-Unc93b1 complex at late endosomes. (**A**) Flag immunoprecipitation of Unc93b1 from Raw264.7 macrophages expressing either WT or non-functional Unc93b1^{H412R} and stimulated for 1 hour with R848 (200 ng/ml) or left unstimulated, followed by immunoblot for Arl8b and TLR7. Representative data of $N = 3$. (**B**) AlphaFold multimer modeling of Unc93b1 and Arl8b. (**C**) Domain structure of Unc93b1 with highlighted mutations. (**D**) Flag immunoprecipitation of Unc93b1 from Raw264.7 macrophages expressing the indicated Unc93b1 mutants and immunoblotting for Arl8b. Representative data of $N = 2$. (**E**) HA immunoprecipitation of indicated TLRs from Raw264.7 macrophages and immunoblotting for Arl8b. Representative data of $N = 2$. (**F**) WT Hoxb8 macrophages were fixed and stained with anti-Lamp1, anti-TLR7, and anti-Arl8b and imaged on a structured illumination microscope. (**G**) Quantification of the colocalization between Arl8b and TLR7 in Borcs7 KO and ctrl Hoxb8 macrophages. Data is expressed as fold-change and pooled from $N = 4$. Each dot presents the average from a single experiment, shaded violin shows the variation of individual cells across all experiments; ratio paired *t* test, two-tailed. (**H**) Quantification of the colocalization between Arl8b and Lamp1 in Borcs7 KO and ctrl Hoxb8 macrophages. Data repeats and analysis as in (G). (**I**) Raw264.7 macrophages expressing Borcs5-GreenLantern were fixed and stained with anti-Lamp1, anti-TLR7, and anti-GFP and imaged on a structure illumination microscope.

mutant allele p.Glu49dup carried a glutamic acid insertion within the N-terminal 5xE acidic patch flanking the ARL8B binding motif thereby extending it to 6xE (Fig. 5, A and B and fig. S6A). UNC93B1 6xE has not been reported in public databases (GnomAD, ExAC, and GME) or in our in-house exome database (5,600 exomes) and thus is a private variant. Phylogenetic analysis of 420 homologous UNC93B1 vertebrate protein sequences encompassing 116 mammalian sequences showed high conservation of the 5xE stretch (Fig. 5C and fig. S6B). No other structural or sequence gene variants associated with SLE (*29*) were identified in the patient genome. UNC93B1 protein levels were comparable in PBMCs from the patient and her parents (Fig. 5D), indicating that the variant did not alter protein expression.

The patient developed progressive autoimmune symptoms at the age of 7, including atopic dermatitis, Hashimotos's thyroiditis, sialadenits, generalized lymphadenopathy, and splenomegaly (Data file S2). At the time of evaluation, the patient exhibited antinuclear antibodies (ANA), leucopenia, massive hypergammaglobulinemia, and complement consumption (Data file S2 and Data file S3). Deep immune phenotyping of PBMCs showed accumulation of total $CD19^+$ B cells, IgD^-CD27^- double-negative (DN) B cells and their $CXCR5^-CD11c^+$ DN2 subset [i.e., age-associated B cells (ABC)], and $CD20^-CD138^+$ plasma cells in the patient, and to some extent in her father, being compatible with increased TLR7 signaling (Fig. 5E and fig. S8) (*30*). $CD24^+CD38^+$ transitional B cells and their $CD10^+CD38^+$ transitional 1 subset, total $CD19^+$ B and naïve $CD21^{low}CD38^{low}$ activated B cells were increased in the patient (fig. S6C). In addition, $CD4^+/CD8^+$ T cell ratio, $CD4^+$ and $CD8^+CD38^+HLA\text{-}DR^+$ activated T cells, and $CD8^+CD57^+PD\text{-}1^+$ exhausted T cells were increased in the patient, and to some extent in her father, reflecting reactive T cell states. In the patient, the $CD4^+CD45R0^+CCR6^-$ helper T cell-derived

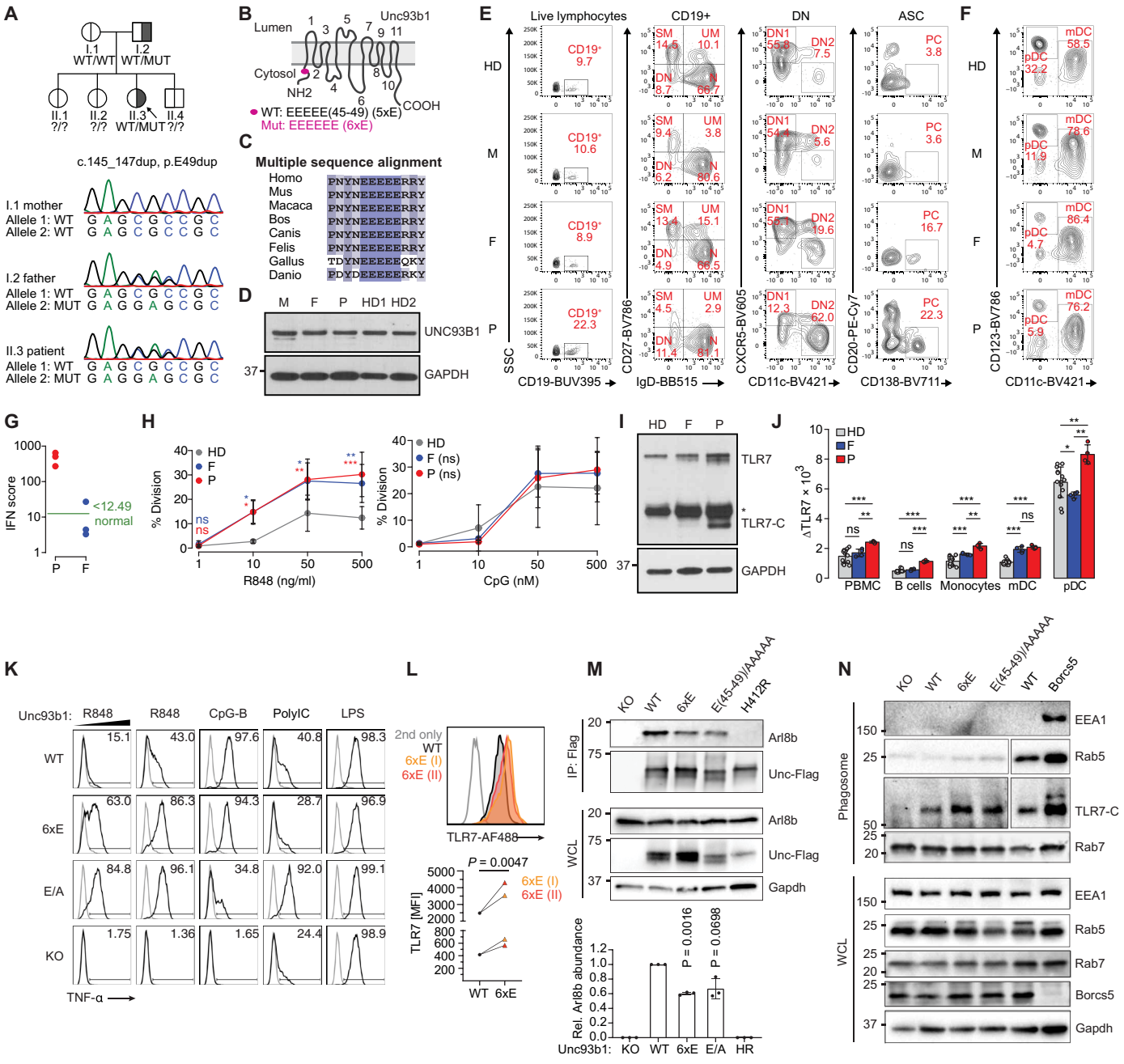

Fig.5. Lupus patient with an Unc93b1 mutation in the Arl8b-binding domain. (**A**) Family pedigree with affected child and Sanger sequencing electropherograms from PBMCs genomic DNA of the patient. (**B**) Domain structure of Unc93b1 with highlighted patient mutation. (**C**) Multiple sequence alignment of the Unc93b1 5xE region. (**D**) UNC93B1 immunoblot from PBMC total protein extracts. (**E-F**) Flow cytometric immune phenotype of peripheral blood from a healthy donor (HD), the patient's mother (M), father (F), and the patient (P). SM: switched memory, UM: unswitched memory, N: naive, DN: double negative, ASC: antibody secreting cell, PC: plasma cell, mDC: myeloid dendritic cells, pDC: plasmacytoid dendritic cells. (**G**) IFN signatures in PBMCs of patient (P) and father (F). An IFN score of 12.49 (dashed green line) indicates the median IFN score of 10 healthy controls plus 2 SD. (**H**) B cell proliferation after titrating TLR7 (R848) and TLR9 (CpG) stimulation of *ex vivo* HD, F and P PBMCs, $N = 3$, two-way ANOVA. (**I**) TLR7 expression by representative western blotting of *ex vivo* bulk primary PBMCs, $N = 3$, and (**J**) intracellular flow cytometry of single cells from HD, F and P, $N = 3$, Welch's *t*-test. (**K**) Intracellular TNF staining of Raw264.7 macrophages expressing the indicated Unc93b1 variants with R848 (5 and 10 ng/ml), CpG-B (300 nM), PolyIC (10 µg/ml) or LPS (25 ng/ml). Representative data of $N = 2$. (**L**) Representative TLR7 flow staining of indicated Raw264.7 macrophage lines. Dot plot shows pooled data from $N = 2$; ratio paired *t* test, two-tailed. (**M**) Flag immunoprecipitation of Unc93b1 from Raw264.7 macrophages expressing the indicated Unc93b1 mutants and immunoblotting for Arl8b. Representative data of $N = 3$. WCL: whole cell lysate. Bar graph shows the quantification of all $N = 3$; ratio paired *t* test, two-tailed. (**N**) Western blot of phagosome preparations. Representative data of $N = 2$. WCL: whole cell lysate.

$CCR4^+CXCR3^-$ helper type 2 (Th2) subset was decreased, reflecting lupus disease activity (fig. S6D) (*31*, *32*). $CD56^+CD57^+$ mature NK cells were reduced and $CD16^+HLA\text{-}DR^+$ pro-inflammatory monocytes were increased in the patient (fig. S6E), while lin^-CD123^+ pDCs were reduced in the patient and her father, reflecting an inflammatory state (Fig. 5F) (*32*, *33*). In line with that, the patient had a highly increased interferon signature, while her father showed intermediate levels (Fig. 5G) (*34*).

To functionally test the impact of TLR7 signaling on primary UNC93B1 6xE cells, we investigated *ex vivo* B cell proliferation after titrating TLR7 (R848) and TLR9 (CpG) stimulation. We found UNC93B1 6xE-bearing cells to start proliferating at suboptimal R848 doses, reaching higher overall proliferation compared to healthy control cells (Fig. 5H and fig. S7). Measurement of TLR7 expression, by western blotting in bulk PBMCs and intracellular flow cytometry in single cells, detected increased TLR7 full length and TLR7 cleaved protein in the UNC93B1 6xE lupus patient compared to the clinically unaffected father with intermediate levels and healthy controls without cleaved TLR7 (Fig. 5I-J and fig. S6F).

As *in vitro* culturing and stimulation of primary UNC93B1 6xE monocytes and pDCs/mDCs showed enhanced apoptosis (fig. S6G) and the accompanying low numbers of pDCs in the patient blood precluded any functional experiments, we further investigated the patient 6xE allele in Raw264.7 macrophages. These cells have been successfully used in the past to dissect TLR7 gain-of-function mechanisms, which then translated well into the development of lupus disease in mice and humans (*10*, *11*). Furthermore, Raw264.7 macrophages as a heterologous expression system also have the advantage of not having been continuously exposed to type I interferons, unlike patient-derived cells, which could potentially confound results by inducing TLR7 upregulation. In response to R848 stimulation, TNF production and *Ifnb* induction were significantly stronger in Raw264.7 macrophages carrying the 6xE variant compared to cells expressing the wild type allele (Fig. 5K and fig. S6H). No differences were observed for TLR9 or TLR3 signaling (Fig. 5K). Unc93b1 KO cells served as negative control. Notably, cells expressing the E/A Unc93b1 mutation showed an even greater response to TLR stimulation, suggesting that the alanine-replacement has a broader functional effect on Unc93b1 than the single E insertion (Fig. 5K). Equal expression levels of the various Unc93b1 mutant variants were validated by flow (fig. S6I). Consistent with our findings in BORC KO cells, we saw an accumulation of TLR7 protein in two independently-derived macrophage lines expressing the patient allele (Fig. 5L), without changes at the *Tlr7* transcript level (fig. S6J). As expected, the additional E insertion reduced the binding between Unc93b1 and Arl8b (Fig. 5M), indicating that the patient allele diminishes BORC-mediated TLR7 degradative sorting into lysosomes, leading to receptor accumulation and increased signaling. We confirmed an accumulation of cleaved TLR7 in phagosomes of 6xE Unc93b1-expressing macrophages (Fig. 5N). As the BORC complex itself was not compromised in these cells, endosome maturation proceeded otherwise normal (Fig. 5N). Our findings demonstrate that interfering with the BORC-mediated homeostatic TLR7 turnover can lead to SLE in humans.

DISCUSSION

Our work highlights the importance of an intact endomembrane system in providing a well-controlled homeostatic turnover of TLR7 to prevent aberrant activation and autoimmune disease. It has been well established that TLR7 gene expression levels must be tightly controlled to avoid excessive stimulation (*5*–*7*, *35*); therefore, mechanisms slowing down the degradation of TLR7 protein would be likewise expected to break self-tolerance. We identified the late endosomal BORC complex as critical component for TLR7-specific degradative sorting, a process important to maintain proper endosomal TLR7 levels and a healthy activation threshold for signaling. BORC deficiency led to an accumulation of endosomal TLR7 in resting macrophages, thereby sensitizing the cell to subsequent activation with RNA ligands.

The lack of any significant effects of BORC on TLR9 signaling might suggest that not all nucleic-acid sensing TLRs are degraded through the same pathway. Experimental evidence has shown that TLR7 and TLR9 take distinct trafficking routes from the ER to endosomes with different regulatory requirements (*36*), making it reasonable to assume that TLR9 traverses different endosomal compartments and is therefore not subject to the BORC-mediated regulation. Our data suggests that Arl8b-BORC engages specifically with TLR7, and that this interaction is required to recruit the more general tethering complex HOPS for mediating lysosomal fusion and receptor turnover. However, Arl8b is not the only endosomal GTPase reported to bind the HOPS complex, as Rab7, another late endosomal GTPase, is able to do so (*37*, *38*). This would suggest that Arl8b-BORC-mediated sorting represents only one out of multiple pathways to degrade membrane proteins in macrophages. This idea is also consistent with our observation that fluid-phase proteolytic probes, such as DQ-BSA, which unrestrictedly enter the endocytic system, display similar degradation kinetics in BORC KO macrophages. Further studies will be required to determine whether, for example, TLR9 would preferentially utilize some of these other lysosomal degradation pathways. Whereas TLR9 was unaffected by BORC, TLR3 signaling showed a slight increase in the absence of BORC, even without a detectable interaction between TLR3 and Arl8b. TLR7 and 3 are targeted to the same endosomal compartments (*39*) and, therefore, it might be possible that some TLR3 passively leaks into the TLR7 degradation pathway. This possibility would also be in line with the greater variability we obtain reading out TLR3 signaling and accumulation.

Interestingly, a Glu49 duplication in Unc93b1, which we identified in a young lupus patient, weakens the interaction between TLR7 and the BORC-Arl8b complex, resulting in reduced degradative sorting and accumulation of TLR7 in late endosomes. The patient allele exists as monoallelic variant, indicating a dominant effect on TLR7 activity. However, the disease penetrance is incomplete, demonstrated by the absence of disease symptoms in the father, who is also a carrier. Incomplete disease penetrance is common for lupus-associated risk alleles, as environmental and (epi)genetic factors are also known to contribute (*40*). Yet, upon closer observation, the father also revealed signs of low-grade inflammation evident by immunophenotyping of PBMCs. Recently, additional families with UNC93B1 mutations in distinct protein regions have been described that also drive lupus disease (*11*). Taken together, these two reports establish a key role for Unc93b1 in preventing excessive TLR7 signaling and autoimmunity in humans.

The involvement of the BORC complex in immune regulation has not been previously described, and might have been obscured by the central role BORC plays in maintaining neuronal integrity. Despite its ubiquitous expression, the BORC-Arl8b complex is particularly important in long-range vesicle transport within axons (*41*). As a result, mice with attenuated BORC function develop progressive

axonal dystrophy and impaired motor function (*42*). Global KO mice of individual BORC subunits or Arl8b are not viable (*22*, *42*–*44*). These animal studies give reason to predict that humans with attenuated BORC function would foremost present with neurodegenerative disorders, which, notably, frequently cooccur with autoinflammatory or autoimmune disease and often share genetic variants and pathways (*45*). This might also explain why no BORC mutations have so far been associated with autoimmune diseases in GWAS studies.

The BORC-Arl8b complex facilitates multiple cellular functions, and we show here that not all cell types utilize these functions equally. In Hela cells and other epithelial cell lines, BORC regulates lysosome positioning and autophagy (*14*, *20*), whereas in macrophages its main role appears to be sorting of endocytic and biosynthetic cargo into lysosomes. The same function seems to apply to dendritic cells, in which Arl8b-deficiency delays lysosomal maturation and cargo delivery to lysosomes, resulting in reduced microbial killing and antigen presentation (*23*). Primary macrophages derived from fetal liver of Borcs7 KO mice also show no difference in lysosome positioning, in agreement with our data (*42*). In TLR7-stimulated plasmacytoid dendritic cells, Arl8b controls the trafficking of TLR7-containing vesicles into the cell periphery for type I interferon induction (*46*), a phenomenon we did not observe in macrophages, presumably due to their general inability to induce type I interferons in response to TLR7 stimulation.

Overall, our work provides an example of how endosomal dysregulation and defective degradative sorting can result in TLR7 gain-of-function and lupus disease in humans. Our findings expand the repertoire of cellular mechanisms important to restrict pathological TLR7 activity and may pave the way for improved treatment through TLR7-targeted precision medicine.

MATERIALS AND METHODS

Study design

The goal of the study was to investigate the role of endosomal BORC in the regulation of nucleic acid-sensing TLRs and their ability to maintain immunological tolerance. The mechanistic part of the study was primarily conducted in various *in vitro* mouse and human macrophage models that had been either engineered with CRISPR-Cas9 or transfected with siRNA to remove various BORC subunits or the associated small GTPase Arl8b. TLR signaling phenotypes were read out via cytokine responses (TNF, IL-8, IFN-beta) by either flow cytometry, ELISA, or qPCR. Endosomal parameters were determined using microscopy techniques and flow cytometry, including endosome positioning, proteolysis, and endosomal pH. Differences in the proteome composition of endosomes from WT and BORC KO macrophages were compared by mass spectrometry analysis of phagosome preparations. Protein mutagenesis and co-immunoprecipitations established an interaction between Arl8b and Unc93b1. In the biomedical part of the study, we describe a pediatric lupus patient with a heterozygous mutation in UNC93B1 that weakens the ARL8b-UNC93B1 interaction. The clinical characterization included immunophenotyping of patient PBMCs, B cell proliferation assays, and Western blot of PBMCs, which together established inflammatory hallmarks of lupus and an accumulation of TLR7 in patient cells resulting in increased B cell proliferation upon TLR7 stimulation. We also expressed the patient UNC93B1 allele in a heterologous mouse Raw264.7 macrophage system to further study the functional role of the mutant allele. Experiments in this study were conducted at least three times unless otherwise specified in the figure legends. No outliers were excluded.

Patients

All subjects and/or their legal guardians gave written informed consent for immunological and genetic investigations that were carried out with approval from the institutional review board of the Ludwig-Maximilians-Universität München (project number 66–14).

Cell and tissue culture conditions

HeLa (DSMZ collection, Germany), HEK293T (ATCC collection) and GP2–293 packaging cell lines (Clontech) were cultured in DMEM (10938–025, Invitrogen) complete media supplemented with 10% (vol/vol) FCS (F0804, Sigma), 1% penicillin-streptomycin (15140122, Gibco), 1% sodium pyruvate (11360070, Gibco), 1% L-glutamine (25030081, Gibco) and 1% HEPES (15630056, Gibco) at 37°C and 5% CO_2. Unc93b1 KO Raw264.7 macrophages (described in (*10*)) and Cas9-expressing Hoxb8 progenitors (described in (*47*)) were a kind gift from the Barton Lab, UC Berkeley. THP-1 cells and WT Raw264.7 cells were a kind gift from the Zychlinsky Lab, MPI for Infection Biology. RAW264.7 and THP-1 cell lines were cultured in RPMI 1640 (31860–025, Gibco) using the same supplements as listed above. The myeloid Hoxb8 progenitors were cultivated in RPMI 1640 medium with 10% FCS, 1% L-Glutamine, 1% Sodium-Pyruvate, 1% HEPES, 1% Penicillin/Streptomycin, 2% GM-CSF-conditioned medium produced by a B16 murine melanoma cell line, 0,0003% β-mercapto-ethanol (21985–023, Gibco) and 0,02% beta-estradiol (Sigma). The Flt3L-derived Hoxb8 progenitors were cultivated in the same media as above, contained 10% Flt3L-conditioned medium produced by a B16 murine melanoma cell line, instead of GM-CSF.

PBMCs were isolated by Ficoll-Hypaque density gradient centrifugation (Biochrom, Berlin, Germany) and cultured in RPMI1640 supplemented with 2 mM Glutamax, 100 U/ml penicillin, 100 μg/ml streptomycin, and 10% FCS (Thermo Fisher Scientific, Waltham, USA) at 37°C and 5% CO_2.

Cell culture and stimulation of human PBMCs

PBMCs were isolated by Ficoll-Hypaque density gradient centrifugation (Biochrom, Berlin, Germany) and cultured in RPMI1640 supplemented with 2 mM Glutamax, 100 U/ml penicillin, 100 μg/ml streptomycin, and 10% FCS (Thermo Fisher Scientific, Waltham, USA) at 37°C and 5% CO_2. For B cell proliferation, PBMCs were labeled with 2.5 μM carboxyfluorescein succinimidyl ester (CFSE, Thermo Fisher Scientific) and stimulated with CpG (ODN 2006, InvivoGen) or R848 (tlrl-r848, InvivoGen, San Diego, USA) for 5 days.

Generation and differentiation of Hoxb8 macrophages

For a detailed description of how to generate Hoxb8 progenitors and differentiate them into macrophages see (*47*, *48*). In brief, for the generation of Hoxb8 progenitors, mouse bone marrow (C57BL/6) was flushed and cultured for 2 days in stem cell medium (DMEM +15% FCS + 25 ng/ml SCF (PeproTech) + 10 ng/ml IL-3 (PeproTech) + 20 ng/ml IL-6 (PeproTech)). Cells were spinfected with retrovirus containing the FLAG-ER-Hoxb8-MSCV-Neo construct and selected for survival/immortalization during subsequent passages in progenitor medium containing beta-estradiol. For the differentiation of Hoxb8 progenitors into macrophages, the progenitor medium was removed by centrifugation at 1200 rpm for 5 min, then the cells were washed twice with 1xPBS. 1 x10^6 progenitor cells were plated in 10 ml

macrophage media (RPMI 1640 medium, 10% fetal calf serum, 1% L-Glutamine, 1% Sodium-Pyruvate, 1% HEPES, 1% Penicillin/Streptomycin, 10% conditioned M-CSF medium produced by a 3 T3 mouse embryonic fibroblast cell line, and 0,0003% β-mercapto-ethanol) in a non-TC treated 10 cm petri-dish. On day 3, 10 ml fresh macrophage media was added. On day 6, 10 ml of the media was exchanged with fresh 10 ml macrophage media. On day 7–9, the macrophages were ready to be used for experiments.

THP-1 differentiation with PMA

THP-1 cells were differentiated for 48 hours using 25 nM PMA (tlrl-pma, Invivogen) in RPMI media supplemented as mentioned above. After 48 hours, the media was removed and cells were washed once with RPMI supplemented media and replaced with fresh media for another 24 hours before stimulation experiments.

CRSPR/Cas9 KO in Hoxb8 progenitors

For a detailed description see (*47*). In brief, Cas9-expressing Hoxb8 progenitors were retrovirally transduced with pLentiGuide Puro (Addgene #52963) in which the gRNA sequences have been cloned using the BsmBI restriction site. gRNA sequences were generated through annealing of two complementary primers with the respective overhangs. 48 hours after spinfection cells were selected with Puromycin in progenitor medium. Used gRNA sequences are listed in the key resource table.

CRISPR RNP Knock-out

Crisprmax Transfection Reagent (CMAX00008, Invitrogen) was used to generate RAW264.7 BORC subunit knock-out cell lines. 1.5 µmol of guide RNA oligos and 1.5 µmol of Alt-R S.p. Cas9 Nuclease v3 protein (1081058, IDT) were mixed with 0.6 µl of Cas9 PLUS reagent in Optimem media to assemble the RNP complexes in a volume of 25 µl. The assembled complexes were mixed with 1.2 µl of CRISPRMAX transfection reagent diluted in 25 µl Optimem and incubated for 20 min at RT. RNP complexes (10 nM final) were transfected into 40,000 cells in a 96-well plastic U-bottom plate. 72 hours post-transfection, cells were single-cell sorted for screening individual knockout clones by Western blot.

Immunofluorescence

Cells were plated onto glass coverslips (No.15H) and allowed to settle overnight. Cells were washed 1x with PBS, fixed with 2% PFA-PBS for 15 min at RT, and permeabilized with 0.5% saponin (Roth)-PBS for 5 min at RT. To quench PFA autofluorescence coverslips were treated with ammonium chloride 50 mM/0.1% saponin-PBS for 10 min at RT. After washing 3x with PBS, cells were blocked in 1% BSA/0.1% saponin-PBS with 4% horse serum (26050–070, Gibco) for 1 hour at RT. Slides were stained in blocking buffer with primary antibodies overnight at 4°C, washed 3x with PBS and incubated for 1 hour with secondary antibodies in blocking buffer at RT. Cells were washed 3x in PBS and mounted using ProLong Glass antifade mountant (P36982, Invitrogen). Cells were imaged on a Zeiss Elyra 7 with lattice SIM with a 63X oil immersion objective.

Superresolution SIM microscopy

Structured Illumination microscopy was performed on the Zeiss Elyra 7 lattice SIM microscope equipped with 405, 488, 561 and 642 nm laser for excitation. Z-stacks from fixed cells were acquired on the SIM mode using a 63X/1.6 oil immersion objective and pco.edge 4.2 sCMOS camera. Raw images were SIM processed and channel aligned using Zeiss default settings in Zen Black. A new channel alignment was acquired for every imaging session, using Hoxb8 macrophages triple-stained for Lamp1 (in AlexaFluor 488, 568, and 647). The calculated off-set from this image was applied to all other images for channel alignment to correct for the shift in xyz between different channels. The completed super-resolution Z-series was visualized and analyzed using Fiji (ImageJ). For image quantification in Cell Profiler individual slices were used. Images for testing antibody specificity were acquired using the wide-field mode. For each new staining panel bleed-through controls were performed with single-stained cells.

Ratiometric fluorescence microscopy

Ratiometric endosomal pH measurements were performed as previously described in (*15*). In brief, VWR confocal dishes (734–2906) were coated with 10 µg fibronectin (F1141, Sigma) on the Ø20 mm glass bottom center, overnight at 37°C. Cells were seeded on freshly-coated plates and loaded with 0.37 mg/mL of FITC-Dextran (Fixable, MW10000, D1820, Invitrogen) and 0.075 mg/ml Alexa 647-Dextran (MW10000, D22914, Invitrogen) overnight. The next day, cells were washed in 1xPBS and incubated with CellMask Orange (1:2000, C10045, Invitrogen) for 10 min at 37°C. Cells were washed again in PBS, taken up in fluoroBrite imaging media (A1896701, Gibco) with 10% FCS + 1% L-Glutamine and imaged on a spinning disk confocal. Confocal microscopy was performed on a Nikon Eclipse Ti2 inverted microscope attached to an Andor Dragonfly 200 spinning disk unit with Andor Zyla sCMOS camera. The microscope was equipped with 405, 445, 488, 514, 561 and 637 nm lasers and operated by Fusion software 2.3. Samples were imaged live using an Apo TIRF 60X/1.49 Oil objective (MRD01691). Analysis see Supplementary Materials.

Imaging of endosome positioning

HeLa cells were plated on 6-well plates and transfected the next day with either 1) Arl8b expression plasmid or empty vector control using Lipofectamine 3000 or 2) siRNA against Borcs5 or scrambled siRNA according to protocol 'siRNA knock down'. After 48 hours cells were fixed and stained with anti-Lamp1, phalloidin-568 (A12380, Invitrogen), and DAPI according to protocol 'Immunofluorescence'. Phalloidin and DAPI served to visualize cell border and nuclei for automated quantification.

Hoxb8 macrophage lines were either stimulated (R848 100 ng/ml) or left unstimulated, and fixed and stained as above. Cells were imaged on a standard spinning disk confocal or laser scanning confocal.

For live-cell imaging, RAW264.7 cells were seeded on fibronectin coated 8-well chamber slides overnight. Next day, the cells were loaded with CellMaskOrange plasma membrane stain (1:2000), LysoTracker Deep Red (1:40000, L12492, Invitrogen) and NucBlue Live Cell Stain diluted in FluoroBrite imaging media (A1896701, Gibco) with 10% FCS + 1% Glutamine for live cell imaging. Analysis see Supplementary Materials.

Immunoprecipitation and Western blot analysis

For Flag-IP: Cells from one confluent 15 cm plate were washed in ice-cooled PBS, scraped and lysed in 1% digitonin lysis buffer (20 mM Tris/HCl pH 7.4, 150 mM NaCl, 1 mM CaCl2, 1 mM MgCl2, 10% Glycerol, 1 × Complete EDTA-free cocktail (11836170001, Roche), PhosSTOP phosphatase inhibitor (04906845001, Roche), 1 mM PMSF (10837091001, Roche) and GTP (2 mM, G8877, Sigma). After a 1 hour

incubation at 4°C on a rotator, lysates were cleared of insoluble material by centrifugation. For immunoprecipitation, lysates were incubated with anti-FLAG matrix (M8823, Millipore; pre-blocked with 1% BSA-PBS for 1 hour) for 2 hours, washed four times in 0.1% digitonin wash buffer (20 mM Tris/HCl pH 7.4, 150 mM NaCl, 1 mM CaCl2, 1 mM MgCl2, 10% Glycerol), and precipitated proteins competitively eluted with Flag peptide (150 ng/µl; F4799, Sigma). Lysates were denatured in SDS-PAGE buffer (4x Lämmli buffer (Bio-Rad) + 20 mM DTT) at room temperature for 1 hour. Proteins were separated by SDS-PAGE (Bio-Rad TGX precast gels) and transferred to Immobilon PVDF membranes (Millipore) in a Trans-Blot Turbo transfer system (Bio-Rad). Membranes were probed with the indicated antibodies and developed using the Licor scanning System (for quantitative western) or the Pierce ECL Plus Western Blotting Substrate (32132, Thermo) and Bio-Rad ChemiDoc imaging system. Samples were normalized based on equal bait protein in eluates, or Gapdh in whole cell lysates.

HA-IPs were performed in the same way, except cleared lysates were incubated with anti-HA matrix (11815016001, Roche) (pre-blocked with 1% BSA-PBS for 1 hour) for 2 hours at 4°C and washed four times and precipitated protein were competitively eluted with HA-peptide (100 ng/ml; I2149, Sigma).

Flow Cytometry

Mouse macrophages were seeded into non-TC treated round-bottom 96-well plates. The next day cells were stimulated with the indicated TLR ligands. To measure TNFα production, BrefeldinA (BD GolgiPlug) was added to cells 30 min after stimulation, and cells were collected after an additional 5.5 h. Dead cells were stained with eFluor 506 or 780 fixable live/dead dye. Cells were blocked with Fc Block anti-Mouse CD16/CD32 (1:200, 101301, Biolegend) for 10 min at RT and then stained for intracellular TNFα with the BD Fixation & Permeabilization kit according to the manufacturer's instruction. Data were acquired on a LSRFortessa or CytoFLEX (Beckman Coulter).

For immune phenotyping, whole blood was antibody stained in brilliant stain Buffer (Becton Dickinson (BD), San Jose, USA) at ambient temperature, lysed with BD Lyse-fix buffer, washed 2 times and live cells were acquired on a BD LSR Fortessa cytometer with FACS Diva software.

B-cell proliferation and differentiation were measured by labeling PBMCs with PC7-anti-CD19 (J3–119, 1:100, Beckman Coulter, Brea, USA), PE-anti-CD27 (L128, 1:25), APC-anti-CD38 (HIT2, 1:12.5), BV421-anti-IgD (IA6–2, 1:100), and 7-amino-actinomycin-D (7-AAD, 2.5 µg/ml, all Becton Dickinson (BD), San Jose, USA). For analysis of TLR7 expression, PBMCs were surface stained with APC-H7-anti-CD3 (SK7, 1:50), BB700-anti-CD14 (M5E2, 1:100), APC-anti-CD56 (NCAM16.2, 1:100), BV711-anti-HLA-DR (G46–6, 1:100), BV421-anti-CD11c (Bu15, 1:100), BV785-anti-CD123 (6H6, 1:100) all BD and PC7-anti-CD19 (J3–119, 1:100, Beckmann Coulter) and intracellular staining was done with PE-anti-TLR7 (S18024F, 1:50, Biolegend) using Cytofix/Cytoperm buffer set from BD. Intracellular staining of cleaved-PARP was performed using Cytofix/Cytoperm buffer set and A647-anti-cleaved-PARP (Asp-214, 1:50) after surface staining with APC-H7-anti-CD3 (SK7, 1:50), BB700-anti-CD14 (M5E2, 1:100), BV711-anti-HLA-DR (G46–6, 1:100), BV421-anti-CD11c (Bu15, 1:100), BV785-anti-CD123 (6H6, 1:100) all BD and PC7-anti-CD19 (J3–119, 1:100, Beckmann Coulter). Sample acquisition was performed on BD FACSCanto II and BD FACSLyric flow cytometer. Data analysis was performed with FlowJo software v10.9.0 (TreeStar, Ashland, USA).

Phagosome preparation

Raw264.7 cells in a confluent 15 cm dish were incubated with ~10^8 magnetic beads (1 µm size, Polysciences) for 4 hours. After rigorous washing in PBS, cells were scraped in 10 ml sucrose homogenization buffer (SHB: 250 mM sucrose, 3 mM imidazole pH 7.4) and pelleted by centrifugation. Cells were resuspended in 2 ml SHB plus protease inhibitor cocktail (Roche) and 1 mM PMSF and disrupted by 20 strokes in a steel dounce homogenizer. The disrupted cells were gently rocked for 10 min on ice to free endosomes. Beads were collected with a magnet (Dynal) and washed 4x with SHB plus PMSF. After the final wash, phagosome preparations were denatured in 2x SDS-PAGE buffer (4xLämmli buffer +20 mM DTT) at room temperature for 1 hour and analyzed by Western blot.

For proteomic analysis, bead-containing phagosomes were additionally washed 4x with ice-cold 100 mM ammonium bicarbonate and snap frozen.

siRNA knock down

Hela cells were plated in a 6-well format. 0.5 µg Plasmid DNA and 2 µM siRNA were diluted in Optimem (3198–062, Gibco) and mixed. 3 µl DharmaFectDuo (T-2010) was diluted in Optimem and incubated for 5 min at RT. DNA/siRNA mixture was added to the diluted DharmaFectDuo and incubated 20 min at RT. The cells were transfected with the complexes and used for assays 48 hours post-transfection. siRNAs were purchased from Dharmacon and are listed in the key resource table.

For THP-1 and Raw246.7 cells, 1.5 µmol siRNA and 0.5 µl Cas9 PLUS reagent were diluted in Optimem. The siRNA was mixed with 0.6 µl of Crisprmax Transfection Reagent (CMAX00008, Invitrogen) diluted in Optimem and incubated for 10 min at RT. 10^5 THP-1 cells or 4x 10^4 RAW246.7 cells in 100 µl were added to the 50 µl transfection mix in a flat bottom 96well (non-TC treated) plate. THP-1 cells were differentiated simultaneously as described earlier. Cells were stimulated 72 hours post-transfection.

Statistics

Statistical parameters, including the exact value of n and statistical significance, are reported in the Figures and Figure Legends, whereby n refers to the number of replicates within the same experiment and N the number of independent experimental repeats. Representative images have been repeated at least three times, unless otherwise stated in the figure legends. Data is judged to be statistically significant when $p < 0.05$. For experiments with two groups two-tailed *t*-test, paired or unpaired was used. Paired *t*-test was used to compare groups from pooled independent experiments, with paired values coming from the same experiment. To compare means of more than two groups, a one-way ANOVA followed by Tukey's multiple comparison test was used. To compare means of different groups across a dose response, a two-way ANOVA followed by a Bonferroni posttest was used. In figures, asterisks denote statistical significance (*, $P < 0.05$; **, $P < 0.01$; ***, $P < 0.001$). Statistical analysis was performed in GraphPad PRISM 9 (Graph Pad *Software* Inc.) or with the software environment R (version 4.3.1).

Supplementary Materials

This PDF file includes:

www.science.org/doi/10.1126/sciimmunol.adi9575
Materials and Methods
Supplementary Text
Figs. S1 to S8

Table S1
References (*49*–*60*)

Other Supplementary Material for this manuscript includes the following:
Data files S1 to S5
MDAR Reproducibility Checklist

REFERENCES AND NOTES

1. N. A. Lind, V. E. Rael, K. Pestal, B. Liu, G. M. Barton, Regulation of the nucleic acid-sensing Toll-like receptors. *Nat. Rev. Immunol.* **22**, 224–235 (2022).
2. S. E. Ewald, B. L. Lee, L. Lau, K. E. Wickliffe, G.-P. Shi, H. A. Chapman, G. M. Barton, The ectodomain of Toll-like receptor 9 is cleaved to generate a functional receptor. *Nature* **456**, 658–662 (2008).
3. S. Maschalidi, S. Hässler, F. Blanc, F. E. Sepulveda, M. Tohme, M. Chignard, P. van Endert, M. Si-Tahar, D. Descamps, B. Manoury, Asparagine endopeptidase controls anti-influenza virus immune responses through TLR7 activation. *PLoS Pathog.* **8**, e1002841 (2012).
4. A. Kanno, C. Yamamoto, M. Onji, R. Fukui, S. I. Saitoh, Y. Motoi, T. Shibata, F. Matsumoto, T. Muta, K. Miyake, Essential role for Toll-like receptor 7 (TLR7)-unique cysteines in an intramolecular disulfide bond, proteolytic cleavage and RNA sensing. *Int. Immunol.* **25**, 413–422 (2013).
5. J. A. Deane, P. Pisitkun, R. S. Barrett, L. Feigenbaum, T. Town, J. M. Ward, R. A. Flavell, S. Bolland, Control of Toll-like receptor 7 expression is essential to restrict autoimmunity and dendritic cell proliferation. *Immunity* **27**, 801–810 (2007).
6. P. Pisitkun, J. A. Deane, M. J. Difilippantonio, T. Tarasenko, A. B. Satterthwaite, S. Bolland, Autoreactive B cell responses to RNA-related antigens due to *TLR7* gene duplication. *Science* **312**, 1669–1672 (2006).
7. S. Subramanian, K. Tus, Q.-Z. Li, A. Wang, X.-H. Tian, J. Zhou, C. Liang, G. Bartov, L. D. McDaniel, X. J. Zhou, R. A. Schultz, E. K. Wakeland, A *Tlr7* translocation accelerates systemic autoimmunity in murine lupus. *Proc. Natl. Acad. Sci. U.S.A.* **103**, 9970–9975 (2006).
8. G. J. Brown, P. F. Cañete, H. Wang, A. Medhavy, J. Bones, J. A. Roco, Y. He, Y. Qin, J. Cappello, J. I. Ellyard, K. Bassett, Q. Shen, G. Burgio, Y. Zhang, C. Turnbull, X. Meng, P. Wu, E. Cho, L. A. Miosge, T. D. Andrews, M. A. Field, D. Tvorogov, A. F. Lopez, J. J. Babon, C. A. López, Á. Gónzalez-Murillo, D. C. Garulo, V. Pascual, T. Levy, E. J. Mallack, D. G. Calame, T. Lotze, J. R. Lupski, H. Ding, T. R. Ullah, G. D. Walters, M. E. Koina, M. C. Cook, N. Shen, C. de Lucas Collantes, B. Corry, M. P. Gantier, V. Athanasopoulos, C. G. Vinuesa, *TLR7* gain-of-function genetic variation causes human lupus. *Nature* **605**, 349–356 (2022).
9. R. Fukui, S.-I. Saitoh, A. Kanno, M. Onji, T. Shibata, A. Ito, M. Onji, M. Matsumoto, S. Akira, N. Yoshida, K. Miyake, Unc93B1 restricts systemic lethal inflammation by orchestrating Toll-like receptor 7 and 9 trafficking. *Immunity* **35**, 69–81 (2011).
10. O. Majer, B. Liu, L. S. M. Kreuk, N. Krogan, G. M. Barton, UNC93B1 recruits syntenin-1 to dampen TLR7 signalling and prevent autoimmunity. *Nature* **575**, 366–370 (2019).
11. C. Wolf, E. L. Lim, M. Mokhtari et al., UNC93B1 variants underlie TLR7-dependent autoimmunity. *Sci. Immunol.* **9**, eadi9769 (2023).
12. A. Ballabio, J. S. Bonifacino, Lysosomes as dynamic regulators of cell and organismal homeostasis. *Nat. Rev. Mol. Cell Biol.* **21**, 101–118 (2020).
13. J. Pu, C. M. Guardia, T. Keren-Kaplan, J. S. Bonifacino, Mechanisms and functions of lysosome positioning. *J. Cell Sci.* **129**, 4329–4339 (2016).
14. J. Pu, C. Schindler, R. Jia, M. Jarnik, P. Backlund, J. S. Bonifacino, BORC, a multisubunit complex that regulates lysosome positioning. *Dev. Cell* **33**, 176–188 (2015).
15. D. E. Johnson, P. Ostrowski, V. Jaumouillé, S. Grinstein, The position of lysosomes within the cell determines their luminal pH. *J. Cell Biol.* **212**, 677–692 (2016).
16. J. P. Caviston, A. L. Zajac, M. Tokito, E. L. F. Holzbaur, Huntingtin coordinates the dynein-mediated dynamic positioning of endosomes and lysosomes. *Mol. Biol. Cell* **22**, 478–492 (2011).
17. C. Erie, M. Sacino, L. Houle, M. L. Lu, J. Wei, Altered lysosomal positioning affects lysosomal functions in a cellular model of Huntington's disease. *Eur. J. Neurosci.* **42**, 1941–1951 (2015).
18. D. Rigante, C. Cipolla, U. Basile, F. Gulli, M. C. Savastano, Overview of immune abnormalities in lysosomal storage disorders. *Immunol. Lett.* **188**, 79–85 (2017).
19. T. Into, M. Inomata, E. Takayama, T. Takigawa, Autophagy in regulation of Toll-like receptor signaling. *Cell. Signal.* **24**, 1150–1162 (2012).
20. R. Jia, C. M. Guardia, J. Pu, Y. Chen, J. S. Bonifacino, BORC coordinates encounter and fusion of lysosomes with autophagosomes. *Autophagy* **13**, 1648–1663 (2017).
21. A. C. Borchers, L. Langemeyer, C. Ungermann, Who's in control? Principles of Rab GTPase activation in endolysosomal membrane trafficking and beyond. *J. Cell Biol.* **220**, e202105120 (2021).
22. C. J. Bell, N. Gupta, K. D. Tremblay, J. Mager, Borcs6 is required for endo-lysosomal degradation during early development. *Mol. Reprod. Dev.* **89**, 337–350 (2022).
23. S. Garg, M. Sharma, C. Ung, A. Tuli, D. C. Barral, D. L. Hava, N. Veerapen, G. S. Besra, N. Hacohen, M. B. Brenner, Lysosomal trafficking, antigen presentation, and microbial killing are controlled by the Arf-like GTPase Arl8b. *Immunity* **35**, 182–193 (2011).
24. J. Anderson, G. Walker, J. Pu, BORC-ARL8-HOPS ensemble is required for lysosomal cholesterol egress through NPC2. *Mol. Biol. Cell* **33**, ar81 (2022).
25. D. Khatter, V. B. Raina, D. Dwivedi, A. Sindhwani, S. Bahl, M. Sharma, The small GTPase Arl8b regulates assembly of the mammalian HOPS complex on lysosomes. *J. Cell Sci.* **128**, 1746–1761 (2015).
26. H. Ishida, J. Asami, Z. Zhang, T. Nishizawa, H. Shigematsu, U. Ohto, T. Shimizu, Cryo-EM structures of Toll-like receptors in complex with UNC93B1. *Nat. Struct. Mol. Biol.* **28**, 173–180 (2021).
27. Y. M. Kim, M. M. Brinkmann, M. E. Paquet, H. L. Ploegh, UNC93B1 delivers nucleotide-sensing toll-like receptors to endolysosomes. *Nature* **452**, 234–238 (2008).
28. O. Majer, B. Liu, B. J. Woo, L. S. M. Kreuk, E. van Dis, G. M. Barton, Release from UNC93B1 reinforces the compartmentalized activation of select TLRs. *Nature* **575**, 371–374 (2019).
29. S. G. Tangye, W. Al-Herz, A. Bousfiha, C. Cunningham-Rundles, J. L. Franco, S. M. Holland, C. Klein, T. Morio, E. Oksenhendler, C. Picard, A. Puel, J. Puck, M. R. J. Seppänen, R. Somech, H. C. Su, K. E. Sullivan, T. R. Torgerson, I. Meyts, Human inborn errors of immunity: 2022 Update on the classification from the International Union of Immunological Societies Expert Committee. *J. Clin. Immunol.* **42**, 1473–1507 (2022).
30. S. A. Jenks, K. S. Cashman, E. Zumaquero, U. M. Marigorta, A. V. Patel, X. Wang, D. Tomar, M. C. Woodruff, Z. Simon, R. Bugrovsky, E. L. Blalock, C. D. Scharer, C. M. Tipton, C. Wei, S. S. Lim, M. Petri, T. B. Niewold, J. H. Anolik, G. Gibson, F. E.-H. Lee, J. M. Boss, F. E. Lund, I. Sanz, Distinct effector B cells induced by unregulated Toll-like receptor 7 contribute to pathogenic responses in systemic lupus erythematosus. *Immunity* **49**, 725–739.e6 (2018).
31. A. Y. Lee, H. Korner, CC chemokine receptor 6 (CCR6) in the pathogenesis of systemic lupus erythematosus. *Immunol. Cell Biol.* **98**, 845–853 (2020).
32. T. Nogimori, Y. Sugawara, M. Higashiguchi, H. Murakami, H. Akita, S. Takahama, S. Tanaka, T. Yamamoto, OMIP 078: A 31-parameter panel for comprehensive immunophenotyping of multiple immune cells in human peripheral blood mononuclear cells. *Cytometry A* **99**, 893–898 (2021).
33. E. Grage-Griebenow, H. D. Flad, M. Ernst, Heterogeneity of human peripheral blood monocyte subsets. *J. Leukoc. Biol.* **69**, 11–20 (2001).
34. G. I. Rice, G. M. A. Forte, M. Szynkiewicz, D. S. Chase, A. Aeby, M. S. Abdel-Hamid, S. Ackroyd, R. Allcock, K. M. Bailey, U. Balottin, C. Barnerias, G. Bernard, C. Bodemer, M. P. Botella, C. Cereda, K. E. Chandler, L. Dabydeen, R. C. Dale, C. De Laet, C. G. E. L. De Goede, M. D. Toro, L. Effat, N. N. Enamorado, E. Fazzi, B. Gener, M. Haldre, J.-P. S.-M. Lin, J. H. Livingston, C. M. Lourenco, W. Marques Jr., P. Oades, P. Peterson, M. Rasmussen, A. Roubertie, J. L. Schmidt, S. A. Shalev, R. Simon, R. Spiegel, K. J. Swoboda, S. A. Temtamy, G. Vassallo, C. N. Vilain, J. Vogt, V. Wermenbol, W. P. Whitehouse, D. Soler, I. Olivieri, S. Orcesi, M. S. Aglan, M. S. Zaki, G. M. H. Abdel-Salam, A. Vanderver, K. Kisand, F. Rozenberg, P. Lebon, Y. J. Crow, Assessment of interferon-related biomarkers in Aicardi-Goutières syndrome associated with mutations in *TREX1*, *RNASEH2A*, *RNASEH2B*, *RNASEH2C*, *SAMHD1*, and *ADAR*: A case-control study. *Lancet Neurol.* **12**, 1159–1169 (2013).
35. Z. R. Newman, J. M. Young, N. T. Ingolia, G. M. Barton, Differences in codon bias and GC content contribute to the balanced expression of TLR7 and TLR9. *Proc. Natl. Acad. Sci. U.S.A.* **113**, E1362–E1371 (2016).
36. B. L. Lee, J. E. Moon, J. H. Shu, L. Yuan, Z. R. Newman, R. Schekman, G. M. Barton, UNC93B1 mediates differential trafficking of endosomal TLRs. *eLife* **2**, e00291 (2013).
37. C. M. Hickey, C. Stroupe, W. Wickner, The major role of the Rab Ypt7p in vacuole fusion is supporting HOPS membrane association. *J. Biol. Chem.* **284**, 16118–16125 (2009).
38. M. L. Jongsma, J. Bakker, B. Cabukusta, N. Liv, D. van Elsland, J. Fermie, J. L. Akkermans, C. Kuijl, S. Y. van der Zanden, L. Janssen, D. Hoogzaad, R. van der Kant, R. H. Wijdeven, J. Klumperman, I. Berlin, J. Neefjes, SKIP-HOPS recruits TBC1D15 for a Rab7-to-Arl8b identity switch to control late endosome transport. *EMBO J.* **39**, e102301 (2020).
39. T. Nishiya, E. Kajita, S. Miwa, A. L. DeFranco, TLR3 and TLR7 are targeted to the same intracellular compartments by distinct regulatory elements. *J. Biol. Chem.* **280**, 37107–37117 (2005).
40. G. C. Tsokos, M. S. Lo, P. Costa Reis, K. E. Sullivan, New insights into the immunopathogenesis of systemic lupus erythematosus. *Nat. Rev. Rheumatol.* **12**, 716–730 (2016).
41. G. G. Farías, C. M. Guardia, R. De Pace, D. J. Britt, J. S. Bonifacino, BORC/kinesin-1 ensemble drives polarized transport of lysosomes into the axon. *Proc. Natl. Acad. Sci. U.S.A.* **114**, E2955–E2964 (2017).
42. J. N. Snouwaert, R. J. Church, L. Jania, M. T. Nguyen, M. L. Wheeler, A. Saintsing, P. Mieczkowski, F. P. M. de Villena, D. Armao, S. S. Moy, D. N. Lorenzo, B. H. Koller, A Mutation in the *Borcs7* subunit of the lysosome regulatory BORC complex results in motor deficits and dystrophic axonopathy in mice. *Cell Rep.* **24**, 1254–1265 (2018).
43. R. De Pace, D. J. Britt, J. Mercurio, A. M. Foster, L. Djavaherian, V. Hoffmann, D. Abebe, J. S. Bonifacino, Synaptic vesicle precursors and lysosomes are transported by different mechanisms in the axon of mammalian neurons. *Cell Rep.* **31**, 107775 (2020).

44. M. Oka, K. Hashimoto, Y. Yamaguchi, S. I. Saitoh, Y. Sugiura, Y. Motoi, K. Honda, Y. Kikko, S. Ohata, M. Suematsu, M. Miura, K. Miyake, T. Katada, K. Kontani, Arl8b is required for lysosomal degradation of maternal proteins in the visceral yolk sac endoderm of mouse embryos. *J. Cell Sci.* **130**, 3568–3577 (2017).
45. Association Between Neurodegenerative Diseases and Autoimmune Diseases. Front. Neurosci. - Research Topic https://www.frontiersin.org/research-topics/7833/association-between-neurodegenerative-diseases-and-autoimmune-diseases#overview, (2018–2019).
46. S.-I. Saitoh, F. Abe, A. Kanno, N. Tanimura, Y. Mori Saitoh, R. Fukui, T. Shibata, K. Sato, T. Ichinohe, M. Hayashi, K. Kubota, H. Kozuka-Hata, M. Oyama, Y. Kikko, T. Katada, K. Kontani, K. Miyake, TLR7 mediated viral recognition results in focal type I interferon secretion by dendritic cells. *Nat. Commun.* **8**, 1592 (2017).
47. A. W. Roberts, L. M. Popov, G. Mitchell, K. L. Ching, D. J. Licht, G. Golovkine, G. M. Barton, J. S. Cox, Cas9$^+$ conditionally-immortalized macrophages as a tool for bacterial pathogenesis and beyond. *eLife* **8**, e45957 (2019).
48. G. G. Wang, K. R. Calvo, M. P. Pasillas, D. B. Sykes, H. Häcker, M. P. Kamps, Quantitative production of macrophages or neutrophils ex vivo using conditional Hoxb8. *Nat. Methods* **3**, 287–293 (2006).
49. V. Redecke, R. Wu, J. Zhou, D. Finkelstein, V. Chaturvedi, A. A. High, H. Häcker, Hematopoietic progenitor cell lines with myeloid and lymphoid potential. *Nat. Methods* **10**, 795–803 (2013).
50. A. E. Carpenter, T. R. Jones, M. R. Lamprecht, C. Clarke, I. Kang, O. Friman, D. A. Guertin, J. Chang, R. A. Lindquist, J. Moffat, P. Golland, D. M. Sabatini, CellProfiler: Image analysis software for identifying and quantifying cell phenotypes. *Genome Biol.* **7**, R100 (2006).
51. J. Vandesompele, K. De Preter, F. Pattyn, B. Poppe, N. Van Roy, A. De Paepe, F. Speleman, Accurate normalization of real-time quantitative RT-PCR data by geometric averaging of multiple internal control genes. *Genome Biol.* **3**, research0034.1 (2002).
52. UniProt Consortium, UniProt: The Universal Protein Knowledgebase in 2023. *Nucleic Acids Res.* **51**, D523–D531 (2023).
53. A. M. Waterhouse, J. B. Procter, D. M. Martin, M. Clamp, G. J. Barton, Jalview Version 2–A multiple sequence alignment editor and analysis workbench. *Bioinformatics* **25**, 1189–1191 (2009).
54. F. Sievers, A. Wilm, D. Dineen, T. J. Gibson, K. Karplus, W. Li, R. Lopez, H. McWilliam, M. Remmert, J. Söding, J. D. Thompson, D. G. Higgins, Fast, scalable generation of high-quality protein multiple sequence alignments using Clustal Omega. *Mol. Syst. Biol.* **7**, 539 (2011).
55. N. A. Kulak, G. Pichler, I. Paron, N. Nagaraj, M. Mann, Minimal, encapsulated proteomic-sample processing applied to copy-number estimation in eukaryotic cells. *Nat. Methods* **11**, 319–324 (2014).
56. I. Gielisch, D. Meierhofer, Metabolome and proteome profiling of complex I deficiency induced by rotenone. *J. Proteome Res.* **14**, 224–235 (2015).
57. L. Martens, H. Hermjakob, P. Jones, M. Adamski, C. Taylor, D. States, K. Gevaert, J. Vandekerckhove, R. Apweiler, PRIDE: The proteomics identifications database. *Proteomics* **5**, 3537–3545 (2005).
58. A. Subramanian, P. Tamayo, V. K. Mootha, S. Mukherjee, B. L. Ebert, M. A. Gillette, A. Paulovich, S. L. Pomeroy, T. R. Golub, E. S. Lander, J. P. Mesirov, Gene set enrichment analysis: A knowledge-based approach for interpreting genome-wide expression profiles. *Proc. Natl. Acad. Sci. U.S.A.* **102**, 15545–15550 (2005).
59. M. Aringer, K. Costenbader, D. Daikh, R. Brinks, M. Mosca, R. Ramsey-Goldman, J. S. Smolen, D. Wofsy, D. T. Boumpas, D. L. Kamen, D. Jayne, R. Cervera, N. Costedoat-Chalumeau, B. Diamond, D. D. Gladman, B. Hahn, F. Hiepe, S. Jacobsen, D. Khanna, K. Lerstrøm, E. Massarotti, J. McCune, G. Ruiz-Irastorza, J. Sanchez-Guerrero, M. Schneider, M. Urowitz, G. Bertsias, B. F. Hoyer, N. Leuchten, C. Tani, S. K. Tedeschi, Z. Touma, G. Schmajuk, B. Anic, F. Assan, T. M. Chan, A. E. Clarke, M. K. Crow, L. Czirják, A. Doria, W. Graninger, B. Halda-Kiss, S. Hasni, P. M. Izmirly, M. Jung, G. Kumánovics, X. Mariette, I. Padjen, J. M. Pego-Reigosa, J. Romero-Diaz, Í. Rúa-Figueroa Fernández, R. Seror, G. H. Stummvoll, Y. Tanaka, M. G. Tektonidou, C. Vasconcelos, E. M. Vital, D. J. Wallace, S. Yavuz, P. L. Meroni, M. J. Fritzler, R. Naden, T. Dörner, S. R. Johnson, 2019 European League Against Rheumatism/American College of Rheumatology classification criteria for systemic lupus erythematosus. *Arthritis Rheumatol.* **71**, 1400–1412 (2019).
60. S. Richards, N. Aziz, S. Bale, D. Bick, S. das, J. Gastier-Foster, W. W. Grody, M. Hegde, E. Lyon, E. Spector, K. Voelkerding, H. L. Rehm, ACMG Laboratory Quality Assurance Committee, Standards and guidelines for the interpretation of sequence variants: A joint consensus recommendation of the American College of Medical Genetics and Genomics and the Association for Molecular Pathology. *Genet. Med.* **17**, 405–424 (2015).

Acknowledgments: We thank the patient and her family for participation in the study. We acknowledge the contribution of the clinical (Veit Grote, MD; Anna-Lisa Lanz, MD; Bärbel Lange-Sperandio, MD), radiological (Marco Paolini, MD), immunodiagnostic (Irmgard Eckerlein; Mayumi Hofmann; Eva Eisl, Raffaele Conca), and genetic (Wendy Aloo; Meino Rohlfs, PhD) teams at the Dr. von Hauner Children's Hospital and of the clinical chemistry team at the Institute of Laboratory Medicine (Peter Eichhorn, MD) both at the University Hospital, LMU Munich, Germany. We thank Noemie Quinson, Ioulia Sampani, Julian Bünting, and Daniel Landsem for assistance with experiments; Sanket Gosavi for protein modeling; Amin Zehtabian for assistance with the image analysis; the Flow Cytometry Core Facility (FCCF) of the German Rheumatism Research Center Berlin (DRFZ) for assistance with cell sorting; Stefan Bauer (University of Marburg, Germany) for sharing bone marrow of TLR7 KO mice; Beata Lukaszewska-McGreal for proteome sample preparation. Thanks to Arturo Zychlinsky and Greg Barton for carefully reading the manuscript. Figures were created with BioRender.com. **Funding:** This work was funded by the Max Planck Society, the German Research Foundation (MA 9812/1–1 to O.M.), a H2020-MSCA-IF Marie Sklodowska-Curie Individual Fellowship (841440 to O.M.), and the International Max Planck Research School (IMPRS fellowship to H.M.). F.H. was funded by the Care-for-Rare Foundation C4R (160073), the Else Kröner-Fresenius Stiftung EKFS (2017_A110), and the German Federal Ministry of Education and Research (BMBF) - German genetic multi-organ Auto-Immunity Network (GAIN) 01GM2206B. M.L.K. was funded by the German Research Foundation grants KFO249 160548243, CRC237 369799452/A11, CRC237 369799452/B21, and the German Federal Ministry of Education and Research (BMBF) 01GM2206C. C.W. was funded by the German Research Foundation grant CRC237 369799452/J and H.E. by the German Research Foundation grant TRR186 278001972 and the Free University Berlin. J.R. was funded by the LMU Munich Foerderprogramm für Forschung und Lehre. **Author contributions:** Conceptualization: HM, OM; Methodology: HM, CS, ELL, TM, JR, MLK, FH, OM; Investigation: HM, CS, OT, TM, JR, CW, MLK, FH, OM; Visualization: HM, CS, TM, JR, CW, DM, OM; Funding acquisition: HE, CK, MLK, FH, OM; Data curation (proteomics): DM; Project administration: OM; Supervision: FH, OM; Writing – original draft: HM, FH, OM; Writing – review & editing: HM, ELL, OT, DM, MLK, FH, OM. **Competing interests:** Authors declare that they have no competing interests. **Data and materials availability:** The mass spectrometry data have been deposited to the ProteomeXchange Consortium via the PRIDE partner repository with the dataset identifier PXD039263 (proteome analysis of ctrl and Borcs7 KO Hoxb8 macrophages) and PXD040042 (phagosome proteomics of WT and Borcs5 KO Raw264.7 macrophages). Uncropped Western blots are provided in Data file S4 and tabulated data underlying the figures are provided in Data file S5. All other data needed to support the conclusions of the paper are available in the main text or the supplementary materials. Requests for key reagents, such as cell lines or plasmids, should be directed to Olivia Majer. These will be shared upon request, accompanied by a Material Transfer Agreement (MTA) from the Max Planck Society, for non-commercial research purposes.

Submitted 30 May 2023
Accepted 22 December 2023
Published 11 January 2024
10.1126/sciimmunol.adi9575

Abstract

One-sentence summary: The BORC complex prevents human autoimmune disease by controlling endosomal TLR7 levels.